# Mitigating the Grid Impact of Megawatt Heavy-Duty Electric Truck Charging

## Simulation-Based Evaluation Using Representative Medium Voltage Distribution Networks

Julian Severrien

Delft University of Technology

TU Delft

# Mitigating the Grid Impact of Megawatt Heavy-Duty Electric Truck Charging

## Simulation-Based Evaluation Using Representative Medium Voltage Distribution Networks

by

Julian Severrien

to obtain the degree of Master of Science
at the Delft University of Technology,
to be defended publicly on Friday January 26, 2026 at 9:30 AM.


| | | |
|---|---|---|
| Student number: | 5117615 | |
| Project duration: | March, 2025 – January, 2026 | |
| Thesis committee: | G.R. Chandra Mouli | TU Delft, supervisor |
| | Dr.M. Cvetkovic, | TU Delft |
| | Dr. Dipl.-Ing. J.L. (Jose) Rueda Torres | TU Delft |


Style: TU Delft Report Style

An electronic version of this thesis is available at `http://repository.tudelft.nl/`.

TU Delft

# Preface

*This thesis was written as part of the Master's program Sustainable Energy Technology at the TU Delft. The research was conducted during the final phase of the Master's program and is part of a larger research project at this university on the integration and electrification of heavy-duty trucks. The work was conducted under the supervision of Gautham Ram Chandra Mouli, with daily supervision from Leila Shams Ashkezari and Manfredo Sartori, who provided guidance and critical feedback that were essential to my research process. Through this research, I gained deeper insights into the challenges posed by the large-scale electrification of transport. Going through this process has improved my understanding of conducting independent scientific research and has provided me with valuable experience at both the academic and personal levels.*

*Julian Severrien*
*Delft, January 2026*

# Abstract

The electrification of heavy-duty transport requires the large-scale integration of Megawatt Charging Stations at highway rest areas and fuel stations. This infrastructure imposes significant challenges to medium-voltage (MV) distribution networks due to their high power demand, clustered charging events and limited predictability. These characteristics could lead to voltage deviations, increased line loading, and additional stress on grid assets. In this study, the grid impact of Heavy-Duty Electric Vehicle (HDEV) charging stations of varying sizes is investigated and the effectiveness of BESS-based mitigation strategies under the constant and different network configurations is evaluated.

Using time-series power flow simulations in MATLAB/Simulink, the impact of unmitigated HDEV charging is analyses in a radial MV distribution network topology. The results show that the dominant limiting factors of HDEV integration are voltage deviations and increased line loading. Upstream transformer loading does not form the bottleneck in the investigated network. To address these impacts, a number of local Energy Management System strategies are evaluated, including heuristic and optimisation-based control.

The results show that with BESS-based mitigation, serving both the charging station operator and grid operator interests, effectively restores network voltage stability and reduces peak power demand at the charging station. Differences in control strategies have shown distinct charging and discharging patterns of the BESS, which affect line loading and transformer utilisation. Heuristic control provides robust peak shaving by reducing active grid power demand, whereas optimisation-based control showed an improved economic performance and smoother voltage regulation, especially when reactive power is used for voltage support. Simulation with multiple charging stations and decentralised BESS control for voltage regulation resulted in unstable network behaviour, highlighting the necessity of a centrally coordinated voltage regulation mechanism.

Overall, this study provides new insights into the trade-offs in BESS-based mitigation strategies in terms of voltage stability, congestion management and BESS operation for the integration of HDEV charging stations. The findings underscore the importance of coordinated control of decentralised assets to ensure reliable grid integration of these multi-megawatt and highly variable loads.

# Contents

# 1 Introduction

Europe has committed to achieving carbon neutrality by 2050, making the decarbonisation of road transport a critical element of the European climate and energy transition goals. While the passenger transport electric vehicle fleet and infrastructure are rapidly expanding, the electrification of heavy-duty electric transport remains a significant challenge. Unlike passenger EVs, heavy-duty electric vehicles (HDEVs) have a substantially higher energy demand and operate over longer distances. For the large-scale integration of HDEVs, megawatt(MW)-scale charging infrastructure will be deployed along the European highways. These ultra-fast charging stations are expected to impose large, unpredictable, and highly variable loads that could significantly impact the stability of the electricity grid. Understanding the potential grid impact of the charging infrastructure is essential for the sustainable integration of HDEVs.

## 1.1. Background

The electrification of Heavy-Duty transport has fundamentally different technical requirements compared to passenger transport. The operation of Heavy-Duty transport is subject to logistical and economic constraints, which require long driving ranges, high payload capacities, and minimal downtime during recharging events. This results in battery capacities ranging from 400 to 800 kWh, depending on the vehicle's application and, thereby, the energy demand per trip [1]. These battery sizes and HDEV operational constraints translate into high charging power requirements.

To comply with the minimal downtime during refuelling, charging times should align with legally mandated rest periods, typically between 30 and 45 minutes. This makes it necessary to have charging power levels of 350 kW up to more than 1 MW [2]. Conventional fast-charging infrastructure, which is used for passenger EVs, is generally limited to charging power levels of 350 kW. This will be insufficient to comply with the requirements of HDEVs. A comparison of the battery sizes and charging power requirements is illustrated in Figure 1.1a and 1.1b.

Megawatt Charging Systems (MCS) are being developed to address these charging power requirements. The MCS standard facilitates charging voltage levels up to 1250 V and currents up to 3000 A [3]. In theory, this could support charging power levels of 3.75 MW. However, present prototypes typically deliver 1-1.5 MW. While MCS complies with the charging power requirements of HDEVs, the connection of such systems to the electricity grid impose significant technical challenges due to the large instantaneous power demand.

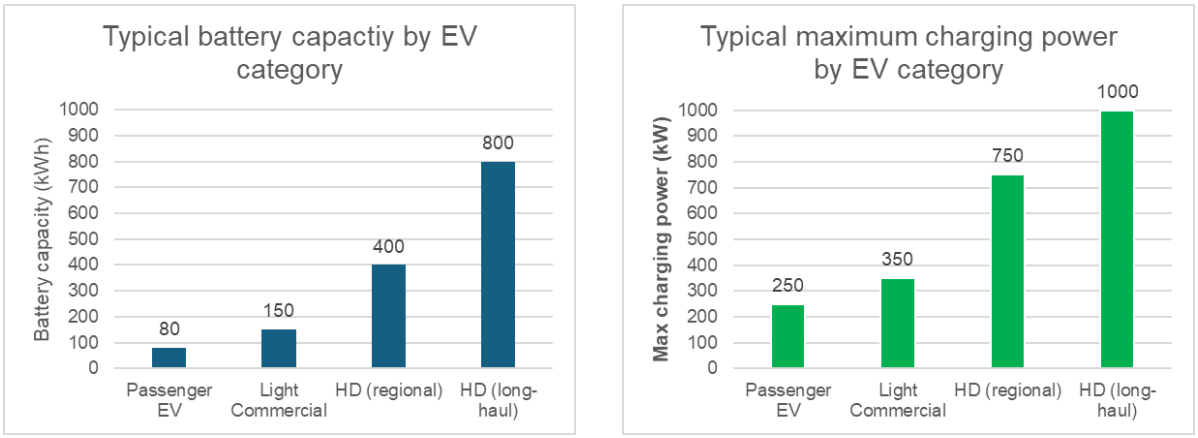


(a) (b)

**Figure 1.1:** Comparison of typical battery capacities (left) and maximum charging powers (right) across electric vehicle categories. Data adapted from [1, 3, 4].

Because of the exceptionally high power requirements of these charging stations, they will typically be connected to the Medium-Voltage (MV) distribution grid. MV grids in Europe range between 1 and 36 kV. These grids are used for both the transport of electricity from the transmission grid to the lower-voltage distribution grid and to large customers. Most MV grids are built with ring structures, which ensure grid reliability during failure events. However, in practice, during normal operations, these grids operate in a radial structure. Figure 1.2 shows this schematically. During normal operation, the NOP(Normally Open Point) and therefore two radial feeders. In this way, the grid is not overloaded, and when failures occur, electricity can be rerouted to ensure the supply within the entire grid.

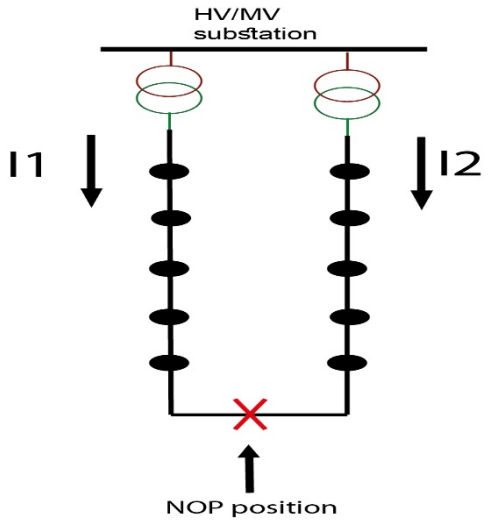


**Figure 1.2:** Schematic overview of a MV grid [5]

With the introduction of HDEV charging stations in a MV grid, the literature consistently identifies the following key challenges:

**Voltage Deviation**

Voltage deviation refers to the reduction or increase in nodal voltage caused by changes in current flowing through the feeder. High-power charging events introduce large currents and often sudden spikes in network load demand [2]. This could lead to immediate voltage drops. This could compromise grid stability. Understanding voltage deviation is therefore essential for grid-impact studies, given regulatory voltage limits and operational boundaries.

The magnitude of a voltage drop is directly related to the currents flowing through the feeder and the impedance of components and lines: higher currents through the feeder cause a greater voltage drop. In simplified form, this relation between current, impedance and voltage drop can be expressed as

$$\Delta V_{i+1} = V_i - I_{i,1+1} * Z_{i,i+1}. \tag{1.1}$$

in which the voltage of the next node is determined by the voltage of the previous node, the voltage drop over the line due to the current flowing through, and the impedance of the line in between. During a high-power charging event, the feeder current increases rapidly, leading to an immediate decrease in nodal voltages. The severity of the voltage drop increases as a load is located farther from a feeder, because longer feeders have longer lines and line impedance increases proportionally with their length.

**Transformer Overloading**
Transformer loading is related to the power flowing through the distribution transformer. Transformers have operational limits below which they can operate safely and reliably, and thermal limits above which overheating, accelerated ageing, and component damage occur. High-power charging exhibits steep load ramps, significantly increasing transformer loading. Therefore, transformer loading is an important factor for HDEV charging stations.

The thermal behaviour of a transformer is strongly affected by its loading profile. High loads on a transformer increase copper and core losses, which result in the accumulation of heat inside the transformer at the windings. Even short periods of high currents can result in significant thermal stress. MCS, particularly with simultaneous sessions, introduces such a high load that it makes the transformer more vulnerable to insulation ageing and thereby reduces its lifetime.

**Grid Congestion**
Grid congestion occurs when the current flowing through the feeder reaches or exceeds its operational or thermal limits. The capacity of an MV network to transport power is limited, and during high-power charging, high load peaks increase the overall load on the system. When multiple HDEVs start charging simultaneously, these peaks add up and could push the feeders to their limits. Therefore, grid congestion plays a key role in the integration of MW charging stations.

The capacity of the feeder is determined by the conductor temperature and the thermal dissipation. As MW-scale charging stations draw large additional currents through the lines, conductor temperature increases, and this effect becomes more severe as more chargers are occupied. Additionally, resistive line losses ($I^2R$) increase with higher currents, thereby contributing to the temperature rise and reducing the usable capacity of the feeder. This includes both the feeder's lines and the upstream substation.

**Stochastic Load Behaviour**
Two load patterns can be distinguished, e.g. depot charging and en-route charging. The demand profile of HDEV charging stations, especially located at highways, rest areas, and fuel stations are characterised by high variability and unpredictable charging behaviour [6]. Unlike passenger EV charging or HDEV depot charging, which occur within specific time windows and result in relatively predictable daily peaks, HDEV en-route charging depends on logistic schedules, range limitations and driving regulations.

As a result, charging sessions take place irregularly throughout the day, with substantial differences in both power demand and duration. This irregularity leads to large, unpredictable fluctuations in the aggregated load profile of such charging stations, including sharp peaks of several MW when multiple chargers operate simultaneously. This makes load forecasting and grid operation increasingly complex, as grid operators cannot rely on consistent or repetitive demand patterns [2].

## 1.2. Problem Statement

As discussed, the electrification of heavy-duty transport will introduce a new class of charging station, which causes severe stress on the grid. While these grid impacts of voltage deviation, transformer overloading and grid congestion are well investigated for passenger EV charging stations, these studies, however, focus on lower power levels, simplified charging profiles and isolated charging stations. Battery Energy Storage Systems, in combination with Photovoltaic generation (PV), are widely proposed as a

mitigation measure. But the performance of these measures in the context of HDEV charging stations remains insufficiently investigated. In particular, clustered charging events, storage operation, and the grid behaviour remain underexplored in the current literature. This limits the ability to determine whether these mitigation strategies can effectively support the large-scale integration of HDEV charging infrastructure.

## 1.3. Objectives and Research Questions

Building on the problem described in the previous section, this study aims to investigate the impact of high-power charging stations for HDEVs and to identify effective mitigation strategies to ensure the reliable and stable operation of MV distribution networks. Dynamic time-domain simulations are used to analyse grid performance under the influence of one and multiple charging stations and to evaluate the effectiveness of various mitigation measures.

**Main Research Question:**

What is the impact of high-power HDEV charging on MV distribution grids, and how can mitigation strategies — such as BESS, Renewable Energy Sources (RES), and Energy Management Systems (EMS) — be applied under centralised and decentralised configurations to reduce this impact?

**Sub-questions**

1. What are the technical impacts of high-power HDEV charging on MV distribution networks in terms of voltage deviation, transformer loading, and network losses?
2. How effective are local mitigation strategies such as PV generation and BESS in reducing grid stress?
3. What is the comparative performance of decentralised versus centralised or hybrid control in improving grid performance?

## 1.4. Scope and Limitations

This study focuses on the assessment of grid impact and mitigation strategies for HDEVs in MV distribution networks. The scope is limited to operational mitigation with BESS, which is enhanced by the generation of a PV system deployed at a charging station. Analysis mainly focuses on network dynamics such as voltage deviations, transformer loading and grid congestion. Frequency stability is not investigated in this study. For computational efficiency, while maintaining sufficient detail to align with the research objective, simplified models for the BESS, PV system, and network loads are used. These capture the power flow interactions and SOC dynamics, while neglecting the detailed component-level behaviour, such as battery degradation. In addition, long-term planning aspects such as grid reinforcement and regulatory considerations are outside the scope of the study. Even though these limitations could restrict the generalisation of the results, the scope of the study is sufficient to evaluate the effectiveness of the investigated mitigation strategies for coping with the grid impact of HDEV charging and add new insights to the existing body of literature about HDEV charging.

## 1.5. Thesis Structure

This thesis is structured into six chapters:

Chapter 1 introduces the topic, providing background information, motivation for the research, the problem definition, research objectives, and the scope of the study.

Chapter 2 presents an overview of the relevant and recent literature on heavy-duty electric vehicle (HDEV) charging, grid impact studies, and mitigation approaches that aim to reduce the adverse effects of large-scale charging loads on distribution networks. Also, the modelling approaches used in the literature are discussed.

Chapter 3 describes the methodology adopted in this study, including the development of a Voltage Sensitivity Matrix, sizing of the BESS and PV system and the development of BESS control strategies and the evaluation criteria for the simulations.

Chapter 4 details the configuration, data, and assumptions of the MV network model, implemented in MATLAB/Simulink, including the network parameters, the charging station implementation, and the integration of mitigation strategies. Additionally, the scenario building and design are discussed with an overview of all the evaluated scenarios

Chapter 5 presents and analyses the simulation results obtained in MATLAB/Simulink for the defined scenarios. The discussion focuses on grid performance indicators, including voltage deviation, power flow, transformer loading, and network losses. In addition, the effectiveness of the implemented mitigation strategies is discussed.

Finally, Chapter 6 summarises the main findings of this study and provides conclusions and recommendations for future research and the large-scale implementation of HDEV charging infrastructure.

# 2

# Literature Review

## 2.1. Grid Impact of HDEV charging

In the field of the grid impact of EV charging, a large number of studies have been carried out, with a small part particularly focused on the impact of HDEV charging. In the literature on the impact of EV charging, 3 significant technical challenges arise with the introduction of EV charging stations, namely: transformer overload, grid congestion and voltage deviations[7]. Even though the studies reviewed focus mainly on "normal" passenger EV charging, these challenges, in other quantities, also arise from integrating HDEV charging. The following subsections discuss these challenges.

#### Voltage deviation

In [2], a grid impact analysis is performed for the HDEV charging station. In this study, HDEVs were defined with a driving range of 400-800 km on a single charge. The investigated charging station was defined as a system with 5 charging points, each with a charging capacity of 1.2 MW. With this setup, a time series analysis is performed with the charging station connected at varying locations, based on the suitability of the connection points. It showed that the introduction of HDEV charging stations in a Californian feeder can lead the nodal voltage to drop to levels of 0.5 p.u. for the worst location, whereas better locations also show drops below 0.85 p.u.

This phenomenon is underscored by [8], which investigated an IEEE 33-bus MV network with charging load data based on charging time, charging power and number of vehicles. This resulted in three charging profiles. The locations of the charging stations varied from close to the main feeder to far from it. They concluded that nodes far from the main feeder will experience voltage drops below the acceptable limit when a multi-megawatt charging demand is introduced.

[9] has investigated multiple strategies for connecting the charging station to the grid, including the connection via a dedicated substation or connection directly to the secondary side of the substation to reduce the impact on other customers. This demonstrated that the charging station coupling to the grid significantly affects the nodal voltage deviations, as a dedicated substation for the charging station shows a much larger hosting capacity before voltage sag limits of 6% are reached. This together highlights that voltage drops are one of the most severe impacts of high-power charging, and that the severity of the impact is location-dependent.

#### Transformer overloading

Several studies have shown that distribution transformers can be overloaded by the charging demand of electric vehicles. However, in the context of HDEV charging, this remains under-investigated. Studies of passenger EVs can provide preliminary insights, which may be exacerbated for HDEV charging. [10] has investigated the influence of EV penetration levels on the thermal loading of distribution transformers. Multiple , and found that with an EV penetration level of 50%, the lifetime of a transformer can be reduced to 1-2 years, from an original 20 years. This is supported by research of [11] in 2011, in which a number of only 10 EVs charging simultaneously decreases the life of a distribution transformer up to 3.5 %.

#### Grid congestion

In the study by [12], several SimBench distribution grids (e.g., rural, commercial, semi-urban, and urban) are analysed for the impact of HDEV charging stations. It investigates a charging station with 7 charging points and 36 night-charging points, combined with the share of HDEVs and their arrival frequency, to model an annual charging profile. Additionally, 3 grid utilisation scenarios are used to represent the increasing normal loads in the network by RES and modern loads such as heat pumps in the future. This study found that in rural grids, line utilisation can reach up to 120%, and almost all line loading can be attributed to HDEV charging, whereas line loading without it reaches only 20%. In this case, the substation transformer loading does not exceed its capacity, reaching only 50% utilisation.

In contrast, the case study in [6] observed an overload of the regional substation's operational capacity. The case study was performed on a Norwegian regional MV grid with 12 buses. With the traffic flow and a varying share of HDEVs, multiple load profiles are constructed. The HPCSs in this area are modelled into a single charging station with sixteen 150 kW outlets and four 350 kW outlets. They have shown that with a share of 25% of HDEVs, the operational limit of the substation is reached, and when the share is increased to 50%, the thermal rating is also exceeded.

## 2.2. Mitigation Strategies

A broad range of mitigation strategies has been explored to address the aforementioned grid impacts of charging stations. However, the body of literature focused on mitigating the impact of HDEV charging remains limited. On the one hand, there are local measures at charging stations, deploying assets such as BESS and PV systems, and distinct strategies for on-site EMSs. On the other hand, the literature proposes network-side mitigation measures, including grid reinforcement and transformer upgrades. The primary focus of this study will be on-site mitigation, as decentralised solutions offer shorter implementation times and are therefore more likely to facilitate the early integration of such charging stations and HDEVs. In the following sections, the most relevant strategies and the corresponding findings in recent studies are reviewed.

### 2.2.1. Grid reinforcement

Grid reinforcements are rarely discussed as an explicit mitigation strategy for the impacts of high-power charging stations in the reviewed literature. Instead, grid reinforcement is mostly treated as a consequence when the limits of the electrical system components, such as transformers and cables, are reached, or voltage violations occur. Many grid impact studies acknowledge these problems, as discussed in the previous section [6, 12].

Although grid reinforcements could be a technically effective strategy to address the aforementioned issues, they require long-term planning and investment rather than providing an operational mitigation measure. Therefore, the implementation of this is not often analysed in detail within EV studies. Additionally, grid reinforcements are often accompanied by a lack of flexibility and can lead to over-sizing when applied to networks with highly variable demand profiles.

### 2.2.2. BESS

Battery Energy Storage Systems are the most commonly evaluated asset for managing the impact of charging stations, as they have the ability to mitigate several types of grid impact, such as voltage deviation and transformer overloading. BESS can release energy during periods of high demand, thereby reducing grid load and mitigating voltage drops and transformer loading. The main benefits of a BESS in the literature are: peak shaving, load smoothing and voltage support. Besides these benefits, BESS is widely studied for supporting the integration of PV generation, congestion management, and capacity enhancement.

#### Forecast-Based Control

Many studies have shown that the controlled charging and discharging of a BESS, based on local grid conditions, can effectively mitigate unfavourable grid conditions. In particular, forecast-based control strategies are frequently applied to achieve peak shaving in distribution networks[13–16]. These methods consistently show a significant reduction of peak grid demand when accurate load forecasts are available.

[13] uses linear regression to forecast the circuit load behaviour. Optimising the weighted total load through the transformer and the cost of SoC determined the BESS output over a time horizon. The weight factor is a quadratic function of the transformer load, penalising high load flow through the transformer. This approach is compared with the use of a reference power curve based on electricity price and renewable energy generation in the objective function. Using a reference power curve showed better results in this

In [14], two approaches for peak shaving and load smoothing are proposed. The first approach includes peak shaving based on forecasted loads, with load smoothing as an add-on function using the BESS's available spare power. The second approach assumes a linear line based on the startup time of rapid generators, around which the BESS levels out the load. With real-time control, the latter provides the best smoothing, with minimal change in SoC.

On the other hand, [15] uses the predicted load in a BESS control algorithm, splitting the day into two timeframes based on the electricity price: one for charging and the other for peak shaving. A net-load threshold determines the BESS's peak-shaving behaviour. Using this strategy showed a significant reduction in overall electricity costs.

A three-layer Model Predictive Control (MPC) scheme using load forecasting is proposed in [16], in which the first layer accounts for economic dispatch with day-ahead forecasts. The second layer accounts for the live operation, trying to achieve the setpoints of the first layer, taking into account operational constraints and grid conditions. A third layer can be employed for ancillary services with the spare power. This approach showed a significant increase in grid performance and daily profits in comparison with rule-based and maximum-capacity control.

**Non-forecasted-Based Control**

In addition to forecast-based approaches, control strategies that are not based on load forecasting have been investigated in several studies [17, 18]. These methods include rule-based or power-threshold-based control, in which exceeding predefined limits, such as voltage or power demand, determines whether the BESS charges or discharges. These strategies are effective in mitigating short-duration power peaks and voltage violations, particularly under fluctuating demand patterns.

[17] employs a control scheme in which the load, PV generation, and SoC are continuously monitored. Under high load, the BESS supplies power to reduce transformer loading, and fluctuating PV generation is compensated by the BESS to stabilise the network. The direction of power transfer and market conditions further determine whether the BESS delivers power to the grid or recharges. In short simulations, it reduced transformer loading from 221% to 83%. In the study of [18], a much simpler control is used, which is based on predetermined power thresholds for charging and discharging. This showed four distinct timeframes in which the BESS is charged, recharged or operates in idle mode. An noticable increase in minimum nodal voltage was observed using this control scheme.

However, the performance of such of these non-forecasted BESS control strategies is often limited by the capacity and SOC of the BESS. As these strategies often respond only when a threshold within the rule-based control is reached, sustainable support can be blocked by insufficient stored energy remaining. Furthermore, these studies describe a static threshold in their BESS control or the use of a simplified network. Therefore, the insights into performance under dynamic load behaviour or clustered charging conditions remain limited.

**EV and HDEV mitigation**

Several studies extend the literature of BESS-based mitigation strategies in the context of EV-charging stations, which locally cause significant stress on distribution networks [16–20]. In these studies, the BESS is commonly decentralised and deployed at the charging station to reduce the station's peak demand and mitigate voltage deviations caused by high charging power. These simulation-based analyses show that a BESS can effectively mitigate the impact of charging stations by limiting the transformer loading and thereby avoiding grid congestion and voltage deviations.

In this body of literature, the majority of the existing work is on passenger EV charging [16, 17, 19]. In these studies of passenger EVs, individual chargers of up to only 350 kW are considered. Even though these studies evaluate the performance of such a system with clustered charging, the charging rates at an HDEV charging station can be in the order of 4 times higher per charging point. This could indicate a significant difference in grid conditions and, thereby, in the operation of a BESS system at a charging station.

[17] employs two charging stations with two charging points with an aggregated maximum power of 300kW for each station. On the other hand, [19] investigates multiple charging parks of eight 350 kW chargers, which is similar to the charging stations used in [16]. For these charging levels, in each of these studies, the deployment of BESS reduced peak demand by a considerable amount.

[20], however, does investigate the performance of a BESS at an HDEV charging station with a maximum power per charging point of 1.2 MW. It demonstrated a significant reduction in voltage deviation, depending on the charging station's location within the network. Still, the analysis is restricted to a single charging station with up to 6 charging ports. It evaluated this across multiple scenarios in which the charging station size, location, and network were varied. does not account for interactions among multiple charging stations or cumulative effects at the network level. As a result, the BESS-based mitigation strategy for clustered HDEV charging remains underexplored.

### 2.2.3. Photovoltaic Integration

In the literature, he combination of a PV system with a BESS is frequently proposed as an integrated system [21]. Stand-alone PV systems can cause the grid voltage to rise and could lead to grid congestion through the injection of power into the grid. In combination with a BESS, such a system can act like a flexible energy source. Thereby, the combination mitigates the impact of PV introduction by absorbing excess PV generation and releasing this energy when needed.

In the context of EV charging, PV is typically not considered as the main mitigation strategy for peak load reduction, but more often as a local extra power generation in addition to a BESS. This is due to the common mismatch between the PV generation and the charging demand. Thereby, PV has a positive contribution to the energy balance of the BESS. Integrating this with a BESS enables a hybrid system to effectively reduce the station's power peaks, while the import from the grid is reduced and the voltage kept within acceptable limits[17, 18, 20].

## 2.3. Modelling Approaches in Grid Impact and Mitigation Studies

In addition to mitigation strategies, existing literature differs in the modelling approaches used to evaluate the grid impact and performance of mitigation strategies. Studies vary in network level used, how load is modelled, and the level of detail applied to the BESS and control strategies. These choices affect the results of different mitigation methods and are therefore a significant aspect in evaluating results.

#### Grid topology

In the existing literature, a wide range of network representations is used, varying in voltage level, detail and component modelling. Studies focused on fast- and HDEV charging often use MV distribution grids [6, 9, 16, 18, 19, 22]. Direct connection to the MV grid is shown to be necessary to accommodate the large power demand. Voltage levels range from 6kV to 33kV in the MV grids used in these studies. [9] used a grid representation that consists of a combination of an MV and an LV grid, whereas other studies [6, 16, 18, 19] only focused on MV grids. The main focus in this body of literature is radial grid topologies.

#### Load and Charging Modelling

In the existing body of literature, a wide range of load profile representations is used. Some studies model the load of each individual charger[23]. Other studies use the aggregated load profile of multiple vehicles or chargers [17, 24]. Aggregated load profiles are more commonly used in the context of grid impact, whereas detailed modelling of individual chargers provides greater insight into the behaviour of the charging station itself.

Another difference lies in the construction of the load profile, which can be either deterministic or stochastic. For example, [20] uses a Monte Carlo simulation to determine the load profiles of its charging station, resulting in a variety of charging patterns. On the other hand, most studies use deterministic load patterns, in which the load is known and does not vary, and they do not account for the stochastic behaviour of en-route charging stations [17, 19].

**BESS and PV Modelling**

Modelling of the BESS plays an essential role in studies assessing the effectiveness of mitigation strategies. The BESS model ranges from highly simplified to detailed representations. Many studies use simplified models in which the BESS is modelled as a controllable power source subject to SOC dynamics. These models neglect the other internal BESS and converter dynamics [17, 20]. This simplification enables efficient simulation. However, this could lead to an overestimation of the achievable performance under realistic conditions.

Control strategies are most often implemented at an aggregated level, where the behaviour of the BESS is controlled by predefined rules, power thresholds, or optimisation objectives [16, 17]. Interaction between the BESS and the network dynamics, which are influenced by changing load behaviour, is often simplified, and coordination between multiple storage units is mostly not modelled in detail.

The PV generation is commonly used in combination with a BESS, primarily as an additional energy source [18, 20]. In these studies, PV systems are most commonly modelled as a generator with predefined generation profiles. The mitigation effect of such hybrid systems is primarily attributable to BESS operation, with the PV system serving as an additional generating device rather than an independent mitigation strategy.

In the reviewed literature, a simplified representation of distribution networks, charging demand, BESS, and PV is commonly used to study grid impact and mitigation performance. Although these modelling approaches provide detailed analysis of component dynamics, they have been shown to be sufficient for capturing network dynamics and power-flow interactions. As a result, most studies prioritise capturing system dynamics while abstracting detailed component-level dynamics that have only a limited impact at the grid level.

**Table 2.1:** Overview of simulation studies

| Reference | EV type / charging power | Network level | Mitigation strategy | Control approach | Key findings | Key limitations |
|---|---|---|---|---|---|---|
| [2] | HDEV / one and five 1.2 MW chargers | 34 bus MV radial | – | – | Voltage deviation depends strongly on location; even a good location cannot handle HDEV charging loads | Only focus on voltage, no mitigation explored |
| [8] | HDEV / – | 33 bus MV radial | – | – | Buses farther from the feeder are more sensitive to large HDEV charging loads | Station size not specified, voltage-only focus, no mitigation explored |
| [9] | HDEV / 1 MW + four 250 kW | 13 bus LV radial | – | – | Hosting capacity increases using a dedicated substation or post-transformer connection | No mitigation explored |

| Reference | EV type / charging power | Network level | Mitigation strategy | Control approach | Key findings | Key limitations |
|---|---|---|---|---|---|---|
| [10] | EV fast / eight 350 kW chargers | MV radial | – | – | Transformer lifetime is strongly affect to the EV charging profile, with high penetration lifetime reduced with 98% | Passenger EV only |
| [12] | HDEV / 7 MCS and 36 NCS | Multiple MV grids | – | – | Voltage and line loading are most critical in rural grids with high HDEV penetration | No mitigation explored |
| [13] | – | Not specified | BESS | Load-forecast optimisation | Peak shaving improves using a reference power instead of weighted load | No EV integration |
| [14] | – | Islanded meshed grid | BESS + Wind | Load-forecast optimisation | Improved load smoothing using generator startup-time-based constraints | Islanded operation, no EVs |
| [15] | – | AC microgrid | BESS + PV | Load-forecast algorithm | 40% peak reduction and 55% energy shaved during high-price periods | Microgrid only, no distribution grid |
| [16] | EV fast / – | 11 bus MV radial | BESS + PV | (E)MPC controller | Improved local grid performance and increased profits | Single station, local scope only |
| [17] | EV fast/ two chargers 300 kW aggregated | AC microgrid | BESS + PV | Rule-based control | Transformer overloading reduction with properly sized BESS | Single station, short simulation horizon |
| [18] | – | 22 bus MV radial | BESS + PV | Rule-based control | 11% peak reduction and 20% loss reduction | Static thresholds, no EVs |
| [19] | EV fast / eight 350 kW chargers | MV radial | BESS | Rule-based control | 44% peak load reduction | Passenger EVs only |
| [20] | HDEV | Multiple MV radial feeders | BESS | PF control, rule-based | Effective mitigation with BESS sizing | No multi-station interaction, no control strategy specified, focus on system sizing |

This literature review has shown that high-power EV charging, particularly in the context of HDEV, can impose significant stress on distribution networks, primarily as voltage deviations, transformer overloading, and grid congestion. While these issues have been well investigated for passenger EVs, their impacts will be more severe for HDEV charging due to higher and more concentrated power demand. As a result, studies on operational mitigation strategies for HDEV charging stations, particularly those involving BESS, are a growing body in the literature.

This thesis will contribute to the existing grid impact and mitigation studies in the context of HDEV charging. Whereas most existing work focuses on passenger EVs, limited charging powers and simplified charging profiles, this study will specifically address high-power HDEV charging, with realistic charging profiles and clustered charging events, and the performance of mitigation measures and strategies. This will address the gaps arising from the limited studies on HDEV charging.

The existing body of literature on HDEV charging focuses on single-station charging scenarios and lags in integrating mitigation measures and in comparing the performance of distinct control strategies. By evaluating the performance of multiple control strategies for a BESS, supported by PV generation, this work will provide new insights into the applicability and limitations of BESS integration at single- and multiple HDEV charging station scenarios. Conducting this analysis with both single- and multiple-station charging provides new insights into existing studies on mitigation and the challenges that arise with the large-scale deployment of HDEVs.

# 3

# Methodology

## 3.1. Research Approach

In this research, a simulation-based approach is chosen to assess and evaluate the technical impact of high-power charging stations for HDEV charging on a MV distribution grid and to test the effectiveness of multiple mitigation strategies. The study is conducted through the development of a dynamic network in MATLAB/Simulink. This software enables time-domain simulations of voltage behaviour, transformer loading, and power-flow dynamics in the distribution grid under various charging demand profiles.

After completing the literature review, the model assumptions and input parameters are defined. This part includes the collection of both residential and industrial load profiles and grid parameters, and the generation of HDEV charging profiles via the generator in [25]. Using this information, a grid model in MATLAB/Simulink is developed to represent a baseline 20-kV radial feeder, with each bus containing a residential load, an industrial load, or a combination of both. For this baseline model, a voltage-sensitivity matrix is computed to determine the strength of each node.

Building on the baseline model analysis, a single charging station is added to the network to assess the impact it has on the grid. Following this impact analysis, several mitigation strategies are implemented, including a BESS, a PV system, and an EMS. The effectiveness of these mitigation strategies is evaluated individually and in combination to build an understanding of the contribution of each measure to mitigating the impacts of the HDEV charging station. A feedback loop is incorporated in the modelling process in which the simulation results of early simulations are used to refine the control strategies and system component sizing. An overview of this general workflow is given in Figure 3.1.

All simulation results are evaluated using a set of Key Performance Parameters (KPIs), including voltage variation, transformer loading and overall line losses. This structured approach enables for a systematic evaluation of how the distribution grid is affected by the introduction of HDEV charging and how well different mitigation strategies perform in reducing this impact. By using a dynamic simulation environment, network behaviour can be captured with varying grid conditions under stochastic charging conditions, which enables a realistic assessment of the technical and operational stability.

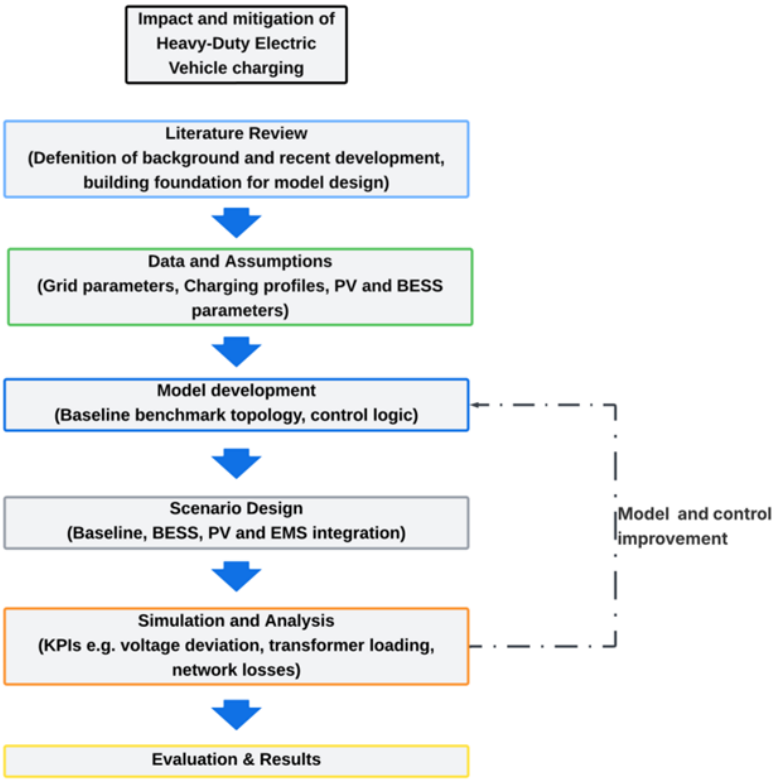


**Figure 3.1:** Overview of the research methodology and simulation workflow.

## 3.2. Voltage Sensitivity Matrix

As discussed in Section 2.1, voltage deviation is one of the biggest challenges in mitigating the impact of HDEV charging. To investigate and properly mitigate the voltage imbalance imposed by such a charging station, a voltage sensitivity matrix is constructed for the grid. The method used to construct the matrix is described by [26]. For 96 timesteps (e.g. every 15 minutes for 1 day), an AC power flow is solved by MATPOWER to model the baseline voltage profile of the network. Additionally, a small increase in load is integrated for each bus $j$, separately for $\Delta P$ and $\Delta Q$, after which a new power flow analysis is performed. The voltage deviation in comparison with the baseline voltage is used to approximate the voltage sensitivities:

$$\frac{\partial V_i}{\partial P_j} \approx \frac{V_{i,\text{pert}}(t,j) - V_{i,\text{baseline}}(t)}{\Delta P_j}, \frac{\partial V_i}{\partial Q_j} \approx \frac{V_{i,\text{pert}}(t,j) - V_{i,\text{baseline}}(t)}{\Delta Q_j} \tag{3.1}$$

Repeating this for all buses and taking the average of over the number of time steps results in two matrices, $VLSM_P$ and $VLSM_Q$. These matrices describe how the voltage magnitude across the network will respond to a change in active and reactive demand or supply. It is assumed that at the operating point of the network(e.g. at base load) the voltage sensitivity behaves linearly. In further equations, the voltage sensitivity obtained from these matrices for a particular node will be denoted $S_{V/P}$ and $S_{V/Q}$. A detailed version of these matrices can be found in Appendix A.3.

## 3.3. BESS and PV Configuration

Two technologies are investigated in this study: a BESS and a PV system. These were integrated into the benchmark network. The purpose of these mitigation strategies is to support the charging station's local power demand, reduce grid import during peak hours, and minimise grid stress through active and reactive power compensation.

### 3.3.1. BESS Modelling

The BESS is modelled as a bidirectional system capable of charging from and discharging to the grid at the MV node where the charging station is connected. The initial battery sizing is performed based on the voltage profile in the baseline scenario, as discussed in Section 4.4. Using this voltage profile across the network and the VSM, the weakest node is selected for the connection of a single charging station. Using the weakest node creates a worst-case assessment of the required battery support capacity.

#### Voltage-sensitivity-based sizing

To estimate the required BESS power, a linearised voltage sensitivity approach is used, in which the node voltage variation is expressed as a function of active power injection and withdrawal:

$$V_i(t) = V_{\text{i,base}} - P_{6,\,\text{station}}(t)\, S_{V/P} + P_{\text{BESS}}(t)\, S_{V/P}, \tag{3.2}$$

where $S_{V/P}$ [p.u./MW] is the voltage sensitivity factor of active power at node $i$ obtained from the voltage sensitivity matrix discussed in the previous section. To maintain acceptable operating conditions, the node voltage is required to satisfy:

$$0.95 \text{ p.u.} \leq V_{\text{next}}(t) \leq 1.05 \text{ p.u.} \tag{3.3}$$

A voltage deviation limit of - 5% is used, as this is the voltage limit most commonly used in grid studies of MV grids[20].

For each time step, the minimum BESS power needed to prevent undervoltage is computed as:

$$P_{\text{BESS,i}}(t) = \max\left(0,\ \frac{P_{\text{grid,i,}}(t)\, S_{V/P} - (V_{\text{i,baseline}} - 0.95)}{S_{V/P}}\right). \tag{3.4}$$

Integrating the required power over the 24-hour period gives the required power the battery must deliver during a daily cycle:

$$C_{\text{BESS, req}} = \int_0^{24\text{h}} P_{\text{BESS}}(t)\, dt. \tag{3.5}$$

#### SoC dynamics

The SoC of the BESS is tracked using an average energy balance model, defined as:

$$E_{BESS}(t + \Delta t) = E_{BESS}(t) + \eta_{\text{ch}}\, P_{\text{BESS,ch}}(t)\, \Delta t - \frac{P_{\text{BESS,dis}}(t)\, \Delta t}{\eta_{\text{dis}}}, \tag{3.6}$$

where $P_{\text{ch}}(t)$ and $P_{\text{dis}}(t)$ denote the charging and discharging powers, and $\eta_{\text{ch}}$ and $\eta_{\text{dis}}$ are the charge and discharge efficiencies (set to 0.95 in this study).

The SoC is defined as:

$$SoC(t) = \frac{E(t)}{E_{\text{BESS}}}. \tag{3.7}$$

Operational constraints of the battery to protect its internal components and lifetime:

$$SoC_{\text{min}} \leq SoC(t) \leq SoC_{\text{max}}, \tag{3.8}$$

with $SoC_{\min} = 0.2$ and $SoC_{\max} = 0.95$. These limits are consequently used in the literature as battery SoC constraints to extend the lifetime of the BESS. Using the SoC limits, the energy bounds in which the BESS operates become:

$$E_{\min} = SoC_{\min} C_{\text{BESS}}, \qquad E_{\max} = SoC_{\max} C_{\text{BESS}}, \tag{3.9}$$

$$E_{\min} \leq E(t) \leq E_{\max}. \tag{3.10}$$

**Power constraints**
The BESS converter is limited by its rated active power:

$$-P_{\text{rated}} \leq P_{\text{BESS}}(t) \leq P_{\text{rated}}. \tag{3.11}$$

and its apparent power constraint:

$$\sqrt{P_{\text{BESS}}(t)^2 + Q_{\text{BESS}}(t)^2} \leq S_{\text{rated}}, \tag{3.12}$$

where for the sizing of the BESS the following is relation is used:

$$S_{\text{rated}} \approx P_{\text{rated}} \tag{3.13}$$

for the calculation of the

### 3.3.2. PV System Modelling

The PV system is modelled as a three-phase current source connected to the same MV node as the charging station, representing an on-site rooftop PV installation. The active power of the PV system is injected at the charging station node as a balanced 3-phase power. The active power output of the PV system is computed using measured irradiance data from the Dutch KNMI dataset, provided by [27]. A representative day in summer is selected: 1 July 2024 for a summer profile to show a distinct difference between with and without PV generation. The available PV surface area corresponds to the estimated rooftop size of a Megawatt Charging Station (MCS) hub. Based on typical dimensions reported by Charging Interface Initiative (CharIN), a charging station with 10 charging points is assumed to provide approximately 1800 $m^2$ of usable PV area [28]. As the main focus of this study lies in the grid impact, the calculation of the power output of the PV system is simplified.

The instantaneous PV power output is computed as:

$$P_{\text{PV}}(t) = I_e(t)\, A_{\text{PV}}\, \eta_{\text{PV}}\, \eta_{\text{conv}}, \tag{3.14}$$

where:

- $P_{\text{PV}}(t)$ — AC active power injected into the grid (W),
- $I_e(t)$ — solar irradiance ($W/m^2$),
- $A_{\text{PV}}$ — installed PV surface area ($m^2$),
- $\eta_{\text{PV}}$ — PV module efficiency,
- $\eta_{\text{conv}}$ — DC–AC conversion efficiency.

In this study, $\eta_{\text{PV}} = 0.20$ and $\eta_{\text{conv}} = 0.97$ are used as typical values for modern commercial systems. In Appendix A.4, two power profiles for this PV system are included for both a winter and a summer day.

### 3.3.3. Grid operation

The net power drawn from the grid is defined as:

$$P_{\text{net}}(t) = P_{\text{load}}(t) - P_{\text{PV}}(t) - P_{\text{BESS}}(t), \tag{3.15}$$

where a positive value of $P_{net}$ indicates power import from the grid. For $P_{load}$, a positive value indicates import from the grid, whereas a positive value of $P_{PV}$ and $P_{BESS}$ indicate an injection of power to the grid.

During periods of high PV generation, the PV power is used first to supply the charging demand and reduce grid import. When PV generation exceeds the instantaneous power demand, the surplus energy is used to charge the BESS when the converter and SoC limits allow it. Conversely, during high-demand or low-irradiance periods, the BESS discharges to support voltage levels, reduce peak loading, or follow the cost-based dispatch strategy. This behaviour of the BESS is coordinated by the EMS. The full control logic governing this interaction is described in Section 3.4.

## 3.4. EMS model

In this study, multiple EMS control approaches are explored stepwise. At first, a heuristic controller is implemented, due to its simplicity and proven ability to mitigate HDEV charging impacts. A price-based incentive for the EMS is used in this study, as the electricity price reflects the grid's supply and demand balance. With this approach, an economically beneficial situation is created for the charging station operator while the mitigation of its grid impacts is ensured. To enhance the charging behaviour of the BESS and the economic performance of the charging station system, this heuristic controller is expanded with an optimiser. The optimiser performs economic dispatch while accounting for current grid conditions and constraints. At this stage, the EMS only regulates the BESS's active power output.

To fully exploit the capabilities of the BESS, the EMS logic is extended to a structure in which active and reactive power are separately controlled, each with a distinct objective: economic dispatch via active power and voltage deviation mitigation via reactive power. After performing simulations for both single charging station and multiple charging station scenarios, the reactive power controller is further developed into a central voltage controller. This central controller provides a single optimisation for each BESS's reactive power output, avoiding grid oscillations caused by individual voltage regulators.

### 3.4.1. Heuristic EMS

At first, a heuristic, rule-based Energy Management System is implemented to coordinate the operation of the BESS and the PV systems at the charging station. The main objective of the heuristic controller is to (i) perform economic dispatch based on average daily prices, (ii) fully utilise the available PV generation, and (iii) mitigate voltage drop due to the high active power demand of the charging station.

The EMS receives as inputs:

- $P_{\text{load}}(t)$; the charging station demand
- $V(i)$; the node voltage
- $\lambda(t)$; the instantaneous electricity price
- $\lambda(:)$; a vector with the daily electricity price porfile
- $SoC(t)$; the state of charge
- $P_{\text{BESS}}(t - \Delta t)$; the BESS power from the previous timestep

#### Control algorithm

The proposed heuristic control strategy consists of two sequential evaluations of the current conditions. On the one hand, the EMS evaluates for the next time step whether it will operate in charge or in discharge mode. On the other hand, it determines if the voltage limits are violated. This prioritises the technical grid requirements while leveraging electricity price variations to support economically beneficial BESS operation, thereby aligning with favourable network conditions. Figure 3.2 shows the flowchart of this heuristic EMS operation.

For price-based operation, the EMS compares the instantaneous electricity price with the average daily electricity price to determine whether the BESS must operate in charging or discharging mode. Low prices indicate strong grid conditions and make charging the BESS favourable, whereas high prices indicate possible grid congestion and push towards shaving of charging loads and enables discharging mode. In charging mode, the BESS charges at its rated power whenever needed, considering the SoC. In discharging mode, the controller determines the discharging setpoint based on the charging station's active load and, when present, PV generation.

For voltage regulation, a baseline nodal voltage is computed at each control interval using the voltage/active power relationship described in Section 3.2. The EMS evaluates whether the voltage in the next time step will exceed the predefined upper or lower voltage limits in the absence of BESS power. To acquire this baseline voltage, the following equation is used:

$$V_{\mathrm{i,base}}(t) = V_{meas}(t - \Delta t) - \frac{-P_{\mathrm{BESS}}(t - \Delta t)}{S_{V/P}}. \tag{3.16}$$

When the upper or lower voltage limit is exceeded, the EMS calculates the corrective BESS power. This calculation is performed with the following equation:

$$P_{\mathrm{BESS,V}} = \frac{V_{i,base} - V_{\mathrm{lim,upper/lower}}}{S_{V/P}} \tag{3.17}$$

For the lower limit, the BESS power used for regulating the voltage is limited to the charging load and is thereby only obliged to mitigate the voltage drops caused by its own load. To prioritise the voltage mitigation for steady grid operation, voltage regulation is prioritised by the ability to override the charge and discharge setpoints when necessary. In operation, the EMS considers the SoC of the BESS in every decision to prevent overcharging and storage depletion.

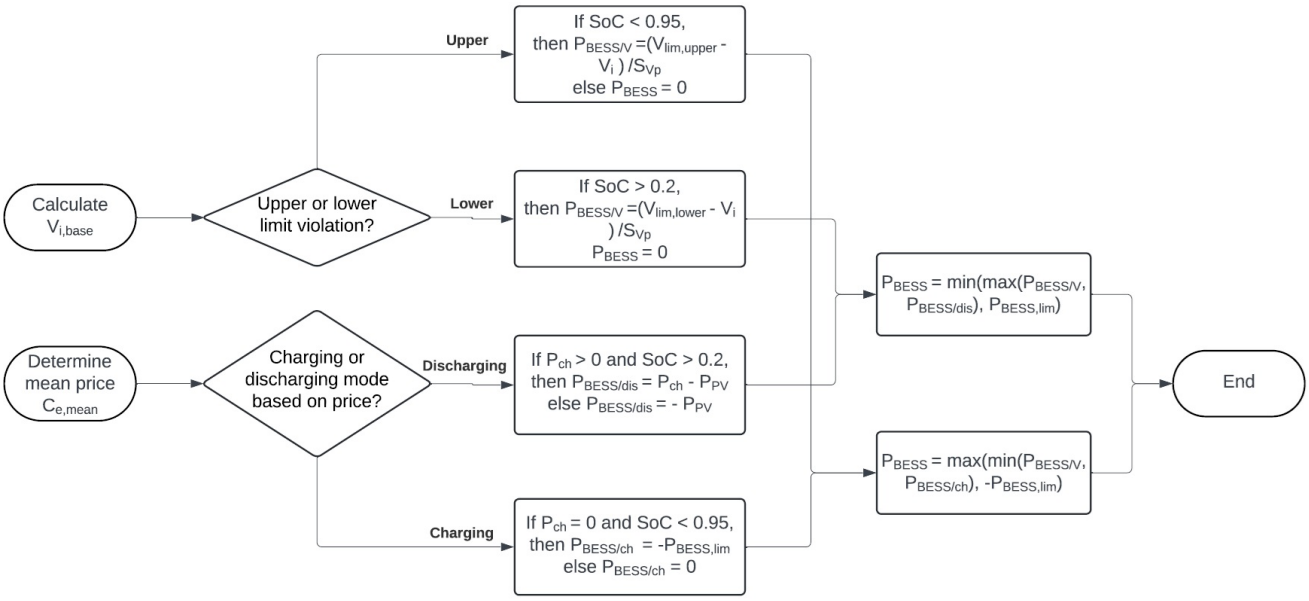


**Figure 3.2:** Flowchart of heuristic EMS

### 3.4.2. Rolling-Horizon BESS Optimisation

As a more comprehensive strategy than the aforementioned heuristic EMS, a rolling-horizon EMS is implemented to control the BESS based on forecasts of load, PV generation, and electricity prices. At each time interval, the controller solves a finite-horizon dispatch problem from time step t until the end of the day. Only the first control action of this horizon is applied to the settings of the BESS, after which the optimisation is repeated at the next time interval.

The optimisation horizon consists of $H$ timesteps. The horizon starts at $t$ and ends at the end of the day($N$), thereby optimising the BESS operation each day until midnight:

$$H = N - t + 1.$$

The EMS receives the same measurement parameters as in the Heuristic controller, but, as this optimiser uses the optimisation horizon, it also receives forecasts in the form of time series from 00:00 to 23:45 for the following parameters:

- $P_{\text{load}}(k)$; the forecasted charging station demand
- $P_{\text{PV}}(k)$; the forecasted PV generation
- $\lambda(k)$; the electricity price

For both the $P_{\text{load}}(k)$ and $P_{\text{PV}}(k)$, at k=1, measurements from the grid are used. For k=2 to $H$, the forecasts are implemented. Because the charging station's load is unpredictable and follows a stochastic pattern, a random day of the year is selected. This forecast is of the same weekday as the simulated charging station load and will serve as a non-perfect load prediction.

**Decision variable and technical constraints**
The optimisation uses the following decision variables over the horizon:

- $P_{\text{ch}}(k)$ — battery charging power (kW),
- $P_{\text{dis}}(k)$ — battery discharging power (kW),
- $SoC(k)$ — battery state of charge (p.u.),
- $P_{\text{grid}}(k)$ — power imported from the grid (kW).

For the technical constraints, the EMS follows the constraints of the BESS, as stated in Section 3.3.1. This includes the SoC dynamics as well as the power constraints. Additionally, an active power constraint is imposed on the BESS to avoid unnecessary export of energy of the BESS to the grid, as competing on the spot market falls outside the scope of this study. This constraint is enforced by:

$$P_{\text{BESS}}(t) \leq P_{\text{load}}(t) - P_{\text{PV}} \tag{3.18}$$

which ensures that power delivered by the PV system is predominantly used to either provide active power to the charging station or recharge the BESS.

For voltage regulation, a voltage constraint is introduced, which enforces the BESS to provide active power when the node voltage drops below the pre-discussed deadband. To calculate the required active power to maintain the voltage above an acceptable limit, the following equation is used:

$$V_{\text{next}}(t) = V_{meas}(t - \Delta t) - \frac{P_{\text{BESS}}(t) - P_{\text{BESS}}(t - \Delta t)}{S_{V/P}} \tag{3.19}$$

on which the EMS enforces the voltage limits stated in Eq. 3.3. This will impose either an upper or lower bound on $P_{\text{BESS}}(t)$, depending on the reached voltage limit.

**Objective**
The objective is to minimise total electricity costs over the horizon, while the EMS encourages the BESS to maintain a sufficiently high SoC at the end of each day. The cost function of the optimiser is given by:

$$\min_{P_{\text{BESS}}(k)} \sum_{k=t}^{N} \Big( \lambda(k)\, P_{\text{grid}}(k) \Big), \tag{3.20}$$

where $\lambda$ is the electricity price in €/kWh, $\Delta t$ is the time step of each time interval. Using this objective function naturally shifts charging towards periods of low prices and low overall demand in the grid, and discharging towards periods of high prices and high overall network demand.

### 3.4.3. Local Voltage Control Through Reactive Power Droop Control

To enable optimal economic dispatch at the charging station using the BESS while maintaining acceptable voltage within its limits, voltage control is decoupled from the BESS's active power dispatch. This avoids unnecessary use of BESS active power for voltage regulation during unfavourable price periods. The BESS converter is equipped with a reactive power droop controller. In this scheme, the economic EMS hierarchically determines the BESS's economic active power dispatch, while the converter's reactive power output is adjusted to support the local voltage at the point of connection.

The controller uses a voltage reference with a deadband $V_{\text{ref}}$, as discussed in Section 3.3.1, and a measured voltage $V_{\text{meas}}$, together with the previously applied reactive power output $Q_{\text{prev}}$. In the reactive power droop controller, a similar linearised voltage sensitivity relation is used as in Eq.3.16 and Eq.3.19, but based on the voltage sensitivity with respect to reactive power injection/extraction rather than active power. This relation is used to determine the base voltage without the impact of the previous output:

$$V_{\text{base}} = V_{\text{meas}} - \frac{Q_{\text{prev}}}{S_{Vq}}, \tag{3.21}$$

where $V_{meas}$ is the measured voltage at node $i$, $Q_{prev}$ the previous reactive power output of the BESS at node $i$ and $S_{Vq}$ the voltage sensitivity factor for reactive power at node $i$ The voltage deviation used by the controller is:

$$\Delta V = V_{\text{ref}} - V_{\text{i}}. \tag{3.22}$$

The previously discussed deadband is applied so that:

$$\text{if } |\Delta V| \leq \Delta V_{\text{db}} \;\Rightarrow\; Q_{\text{target}} = 0, \tag{3.23}$$

For deviations exceeding the deadband, only the excess voltage outside the deadband is used to compute a target reactive power, to avoid excessive use of reactive power.

$$\Delta V_{\text{eff}} = \begin{cases} \Delta V - \Delta V_{\text{db}}, & \Delta V > 0, \\ \Delta V + \Delta V_{\text{db}}, & \Delta V < 0, \end{cases} \tag{3.24}$$

$$Q_{\text{target}} = S_{Vq}\, \Delta V_{\text{eff}}. \tag{3.25}$$

where $S_{Vq}$ is the voltage sensitivity for reactive power injection. The reactive power is further constrained by the converter's apparent power rating. Based on this rating and the converter's active power output, the reactive power output is determined. This imposes a hierarchy within the controller, with the BESS operator's first objective being economic dispatch, followed by voltage control. This limit for reactive power is computed as:

$$Q_{\text{max}} = \sqrt{S_{\text{max}}^2 - P_{\text{ref}}^2} \tag{3.26}$$

The target value of the reactive power droop controller is constrained by this limit as:

$$|Q_{target}| \leq Q_{max} \tag{3.27}$$

### 3.4.4. Central Voltage Control

Simulation with multiple charging stations in the network showed that purely local droop control leads to unwanted interactions among BESS outputs. When multiple EMSs attempt to correct the same voltage deviation, they may overcompensate, causing oscillations in the grid's reactive power flow. To avoid this behaviour, a centralised reactive power controller is implemented in the network that determines the optimal setpoints for each converter, taking into account each converter's available apparent power.

At each time step, the controller receives the following input:

- $V_{\text{i}}(k)$the measured nodal voltages
- $V_{ref}$ the voltage reference
- $P_{BESS,i}$ the active power setpoints of the converter at each charging station
- $S_{max,i}$ the apparent power ratings of each converter
- $Q_{prev,i}$the previously applied reactive power from each converter a list of "weak" nodes where voltage constraints will be enforced

As in the droop controller described in the previous section, this controller makes use of the linear relation between reactive power injecting of nodal voltages, approximated with the sensitivity matrix, as stated in Section 3.2:

$$\Delta V \approx K\,\Delta Q \tag{3.28}$$

where $K$ the voltage sensitivity matrix, constructed as stated in Section 3.2. The uncompensated base voltage is computed for every node by removing the impact of previously applied reactive power using the voltage sensitivity matrix:

$$V_{\text{base}} = V_{\text{meas}} - H\,Q_{\text{prev}}. \tag{3.29}$$

For this controller, the same dead band is used as in Section 3.4.3, described with 3.24. The available reactive power of each converter is limited by the apparent power rating of each converter and its active power setpoint, computed with Eq.3.26

The objective of this controller is to keep the voltage of all monitored nodes, in this case weak nodes, within the predefined deadband while using as little reactive power as possible. Additionally, it distributes reactive power support among converters that are most effective for voltage control at a particular node with voltage violation. To achieve this, a weighted quadratic objective is defined:

$$J_Q = QQ^\top W, \tag{3.30}$$

This quadratic objective meets two desired results:

- it penalises large reactive power outputs, and therefore ensures a smooth operation and efficient droop control
- it naturally distributes the required reactive power output over the converters and thereby avoids large $Q$ setpoints for individual converters

To account for differences in voltage sensitivity across the network, a diagonal matrix $W$ is constructed. This matrix is built up using sensitivity-based weights:

$$S_i = \sum_{i \in \mathcal{B}_{\text{weak}}} |H_{ij}|, \tag{3.31}$$

where $S_{V,i}$ reflects how strongly the $j$-th station affects the weak nodes. Stations with high sensitivity receive a lower penalty, while stations with low sensitivity receive a higher penalty. The weights are calculated as:

$$w_j = \frac{1}{\exp\big(\beta(S_{Vq,i,j} - \max(S_{Vq,i}))\big)}, \tag{3.32}$$

where $\beta$ can be tuned to determine the spread across stations and $S_{max,j}$ is the maximum voltage sensitivity on a particular weak node. This creates a preference for stations with larger converters closer to the weak nodes, and penalises stations with smaller converters and being farther away from the weak bus.

The final optimisation problem to determine the optimal reactive power dispatch over the charging station is defined as:

$$\min_{Q} \quad Q^\top W Q \tag{3.33}$$

$$\text{s.t.} \quad V_{\text{low}} \le V_{\text{base}} + H\,Q \le V_{\text{high}}, \tag{3.34}$$

$$-Q_{\max} \le Q \le Q_{\max}. \tag{3.35}$$

## 3.5. Evaluation Criteria

To evaluate the technical and operational impact of HDEV charging stations and the effectiveness of the proposed mitigation strategies, each simulation scenario is evaluated using a consistent set of Key Performance Indicators (KPIs). These criteria reflect on both grid performance and charging station behaviour, which is directly related to the research objectives described in Chapter 1. These KPIs directly arise from the by literature-appointed impacts.

**Voltage Balance**
For weak nodes across the network, the following voltage metrics are computed:

- Voltage profiles $V_i$: voltage profiles over a day
- voltage limit margin and duration: How deep are the voltage dips, and what is the duration of these dips below the limit

**Transformer and Line Loading**
For overall network performance, the following KPI's will be evaluated:

- Transformer loading $S_{station}$: charging station apparent power demand over a day
- Line loading $I_{line}$: loading of primary line over a day
- Substation loading $S_{sub}$: apparent power of the feeder's substation

**BESS performance**
For the evaluation of the BESS, there are two KPIs most important:

- BESS active power $P_{BESS}$: discharging/recharging behaviour of the BESS
- BESS Throughput: How much energy is charged and discharged over a day

# 4

# Model Setup

## 4.1. Data and Assumptions

The grid topology used in this study is based on the CIRGE European Benchmark Medium-Voltage distribution grid, which represents a typical 20 kV radial feeder, which is shown in Figure 4.1. This benchmark network is designed for comparative grid studies for European applications [29]. The grid includes a mix of residential and industrial loads distributed along underground cables.

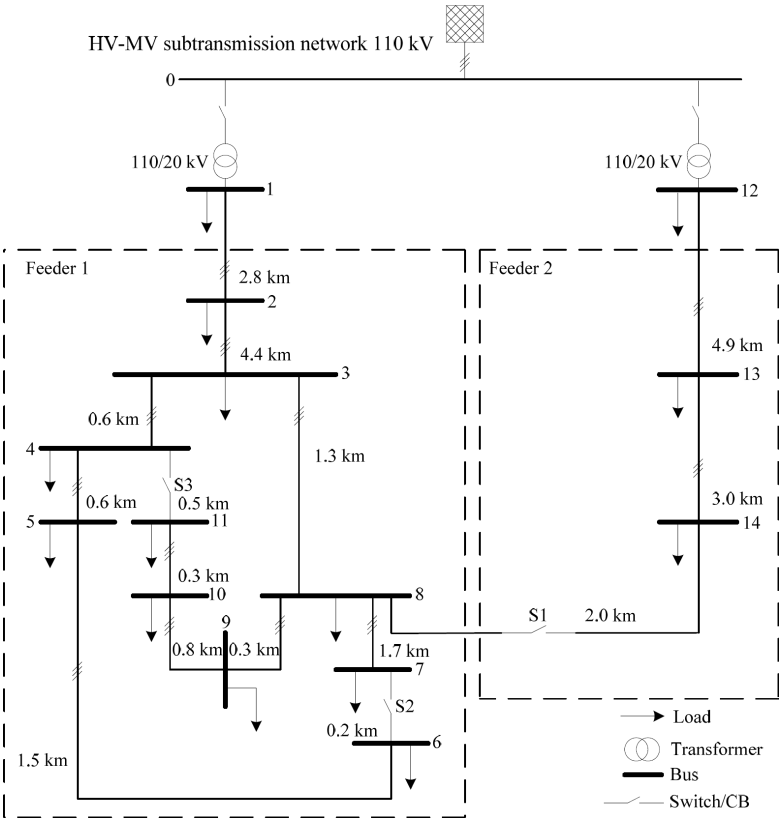


**Figure 4.1:** Grid topology of CIGRE European Benchmark Medium Voltage network [29]

The 14-bus topology has two main feeders connected to a 110kV sub-transmission grid via 110/20kV transformers. Because feeders 1 and 2 are physically disconnected via Switch 1, this study's main focus will be on feeder 1. Table 4.1 shows the system parameters originating from [29], used to build the network in MATLAB/Simulink.

**Table 4.1:** Main parameters of the CIGRE European Benchmark MV distribution network [29].

| Parameter | Symbol | Value / Unit |
|---|---|---|
| Nominal system voltage | $V_{nom}$ | 20 kV |
| Primary transformer rating | $S_{tr}$ | 25 MVA (110/20 kV) |
| Primary transformer connection | - | 3−ph Dyn1 |
| Number of nodes | — | 14 |
| Cable type Feeder 1 | — | NA2XS2Y 120 mm$^2$ (underground) |
| Cable resistance (underground) | $R_{ph}$ | 0.501 Ω/km |
| Cable reactance (underground) | $X_{ph}$ | 0.716 Ω/km |
| Base frequency | $f$ | 50 Hz |

Each feeder is modelled as three-phase branch segments based on data for a standard XLPE underground cable from CIGRE[29]. The impedances per kilometre are taken for each segment and scaled according to the cable lengths, as shown in Figure 4.1. The transformer model in Simulink is a three-phase unit with two windings and a Dyn connection. Both primary transformers are connected to a voltage source of 110 kV, representing the connection to the sub-transmission grid.

### Load profiles

The base load in the grid is a combination of aggregated residential and industrial load profiles. The original load data for each bus in [29] are based on peak apparent power, a power factor, and two normalised load curves for residential and industrial loads. A detailed table of the nodal apparent power and power factor values used for the benchmark network is listed in Appendix A.1. Using these two load profiles for each bus, a combined load profile is constructed. The data of the industrial and residential load curves used in [29] are not publicly available. Therefore, publicly available load curves from [30] for both the residential and industrial normalised load curves are used in this study. Using these real-world data from [30] for constructing the load curves makes the study more representative.

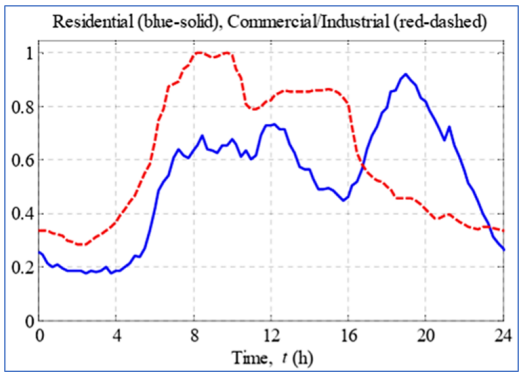


**(a)** Residential and industrial load curves CIGRE [29]

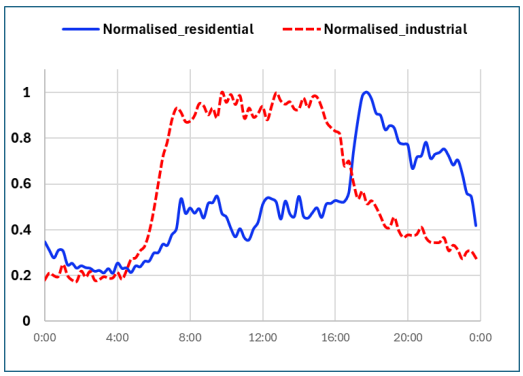


**(b)** Residential and industrial load curves Liander [30]

### Charging profiles

To model the variability of charging demand, stochastic charging profiles are generated using the publicly available charging profile generator in [25]. This generator enables the generation of yearly charging profiles for either a number of charging points or vehicles. Parameters that can be tuned include vehicle type, simulation year, charging location, and charging rate. An extensive explanation of the method used to develop this generator is provided in [25]. Table 4.2 shows the parameter input used to generate the charging profiles used in this study. Multiple charging profiles are used to evaluate the impact difference between a charging station with 5 charging points and one with 10. Additionally, multiple charging profiles are generated with different seeds to enable simulation with multiple charging stations present in the network, each with an individual charging profile. The charging capacity of each charging point is chosen to be 1000 kW, to accommodate the limited downtime during charging, as mentioned in Section 1.1. A yearly charging profile for 5 and 10 charging points can be found in Appendix A.2.

**Table 4.2:** Generator input parameters

| Parameter | Value |
|---|---|
| Profile type | Charge point |
| Number of charging points | 5 / 10 |
| Simulation year | 2035 |
| Location type | Truck parking |
| Charging capacity | 1000 kW |
| Smart charging | Off |
| Random seed | 120 / 121 / 123 |

#### Site Selection

To determine the initial location for connecting the HDEV charging station to the MV-grid, an analysis is performed on the baseline scenario (details of the scenarios can be found in Section 4.4). The voltage profile is combined with the voltage sensitivity factor to evaluate the strength of each node and the likelihood that the voltage limits will be exceeded when an extra aggregated load of a charging station is introduced. The voltage profiles are shown in Section **??** and voltage sensitivity matrices in Appendix A.3. From this analysis, two nodes emerged, namely nodes 6 and 11, with both experiencing similar high-voltage sensitivity factors. Due to the voltage profile of node 6, which showed lower overall voltages than node 11, the decision was made to connect the HDEV charging station in the single-station scenarios (see Section 4.4) to node 6.

## 4.2. Simulink model

#### Load model

At each node, one or multiple loads are present, representing residential and commercial/industrial consumers. The apparent power rating and power factor are listed in AppendixA.1. The normalised load profiles for residential and commercial/industrial loads are presented in Section 4.1. These parameters are used as direct inputs to construct the load profiles in Simulink. As described in Section 4.1, the load profiles for both residential and commercial/industrial are constructed through a combination of the normalised load profile, provided by Liander and the peak apparent power of each load, from the table in Appendix A.1. By combining the load profiles with the nominal voltage (20kV) of the grid, a profile of $\hat{I}$ is constructed with the equation:

$$\hat{I} = \frac{S\sqrt{2}}{V\sqrt{3}} \tag{4.1}$$

The MATLAB script used to compute the current profiles for each load is provided in Appendix B.1. To ensure smooth behaviour and a realistic representation in the grid, the current profile is interpolated between time intervals. As Simulink shows a lot of flicker in the simulation when constant power load blocks are integrated, controlled current sources are used instead. These controlled current sources are fed with a current magnitude for each phase, computed by the Three Phase Sine Generator. For both residential and industrial loads, the sine waves are computed and summed.

#### Simulation configuration

The MV-grid is implemented in Simulink using Simscape Electrical with a discrete-time solver. The following settings are used throughout the simulations:

- Simulation horizon: 24 hours
- Solver: ode3
- Solver timestep: 1e-4 seconds
- Sampling time EMS: 15 minutes/45 seconds (depending on EMS)
- Base voltage: 20 kV (phase-to-phase)

**Time scaling**
To reduce the computational cost of simulating a full 24-hour cycle, a time-scaling factor is applied to the dynamic model. The electrical system in Simulink is simulated in real time with the fixed solver time step mentioned above, while the external time series (e.g., residential and commercial/industrial loads, charging station demand, PV generation, and electricity prices) are compressed in time. A scaling factor of 225 is introduced so that 4 simulated seconds corresponds to 15 minutes of real-world operation. All external inputs are resampled according to:

$$t_{sim} = \frac{t_{real}}{225}$$

which ensures that the power system's dynamic behaviour remains physically accurate, while longer-time-scale variations can be evaluated within shorter simulation times. The operation of the EMS is scaled consistently so that the number of time intervals is consistent with the real-world number of time intervals over a 24-hour cycle. The scaling factor of 225 is chosen through testing to preserve fast-acting electrical transients while drastically reducing simulation runtimes.

**Charging station model**
As stated in Section 4.1, the HDEV charging station is connected to node 6 for analysis of single-station scenarios. The charging station is modelled the same as the other loads in the network: constructing the $\hat{I}$ profile, generating sine waves, and feeding them into the controlled current sources for each phase. In contrast to the network's normal loads, the load of a charging station is modelled without interpolation between time intervals. Through this, the high ramp rate and instantaneous multi-megawatt demand are simulated.

## 4.3. Mitigation Assets

**BESS**
The BESS is modelled to represent its electrical behaviour while ensuring flexible integration with an EMS. Similar to the other loads in the grid, the BESS is connected to the grid through three Controlled Current Sources, one for each phase. The current sources are controlled by a MATLAB Function Block that computes the phase currents required to compute the active and reactive power output of the BESS. Within the block, the setpoints for both active and reactive power are converted into sine waves using the voltage magnitude and phase angle. This ensures that the injected or extracted power corresponds to the setpoints while maintaining synchronisation with the grid.

The setpoints for both the active and reactive power are generated in separate function blocks. For the active power control, a MATLAB-based solver is invoked from within Simulink to compute either the heuristic control or the optimal power dispatch, depending on the scenario simulated. The computation of this solver is performed outside the Simulink environment, but the results are fed back into the function block in real time.

The reactive power control follows one of two modes, depending on the simulated scenario and the EMS configuration: a local droop controller integrated into the BESS system that computes the required $Q$ based on local voltage measurements, or a $Q$ setpoint determined by a central controller outside the BESS. In this way, the grid model, optimisation and control logic, and the physical representation of the BESS are clearly separated, enabling easy integration of multiple EMS strategies.

The MATLAB code used to invoke and execute the EMS logic in each function block is provided in Appendix B. For both the EMSs, the Gurobi optimisation application is used to compute the optimisation problems.

**Photovoltaic System**
As for the loads in the network, the PV system is modelled as a three-phase controlled current source. The injected power follows the PV power profile, calculated in Section 3.3.2. The PV systems is connected to the same node as the charging station and the BESS to enable direct reduction of net grid demand at that node. The PV forecast is also provided to the BESS controller so that power dispatch can account for available PV power throughout the day. This provides a simple, but consistent representation of PV generation and its connection to the MV grid.

## 4.4. Scenario Design

This section gives a description of the simulation scenarios used to evaluate the impact of high-power charging stations and the effectiveness of the proposed mitigation strategies. These scenarios are designed to systematically compare different charging station sizes, numbers of charging stations, locations, and mitigation and control strategies under identical grid and load conditions.

#### Scenario Framework

All scenarios are based on the CIGRE European medium-voltage benchmark network, described in Section 4.1. The grid parameters and residential and industrial load profiles remain identical across each scenario; only the presence and configuration of the charging stations and their mitigation systems are varied.

The scenario framework consists of four levels:

1. **Base scenario**: grid without any charging station
2. **Single Station Scenarios**: a single station is connected to a weak node in the grid, with different sizes and mitigation strategies
3. **Multi-Station Scenarios**: multiple charging stations are connected to the grid, with one size and varying mitigation coordination
4. **Meshed Grid Scenarios**: meshed grid to evaluate the performance of the mitigation strategy under new network conditions, with multiple charging stations at three different locations in the network

This ensures a stepwise analysis: from a fundamental analysis of the grid impact of one station, to the evaluation of mitigation strategies and finally the analysis of the interaction between multiple stations.

#### Base Scenario: MV-grid without HDEV Charging

The base scenario represents the operation of the CIGRE MV-grid without an HDEV charging station. Only the original residential and industrial loads are connected as described in Section 4.1. Further, no BESS, PV or control systems are present.

This scenario serves as a reference for voltage profiles, transformer loading and grid losses. All the upcoming scenarios are evaluated with respect to this base scenario by comparing the nodal voltages, active and reactive power through the feeder and power losses through the lines.

#### Single-Station Scenario

In the single-station scenario, a single HDEV charging station is connected to node 6, which is identified as one of the network's weakest nodes. Two sizes of charging station are considered:

- **5 charging points**: Charging station with 5 charging points of 1 MW with a nominal connection capacity of 4 MVA
- 10 charging points: Charging station with 5 charging points of 1 MW with a nominal connection capacity of 8 MVA

The following configurations are considered, with the station size set to 5 charging points, used only in configurations 1 and 2.

1. **No Mitigation (Scenario S1/S3):**
   The charging station is directly connected to the MV node without any mitigation. This quantifies the uncompensated impact of the HDEV charging station on the network.

2. **BESS-only Mitigation (Scenario S2/S4):**
   A BESS is implemented at the same node as the charging station. For each size, the BESS is dimensioned according to Section 4.1 and controlled by the heuristic EMS described in Section 3.4, which provides rule-based peak shaving, and voltage support through active power compensation.

3. **Hybrid PV-BESS Mitigation (Snecario S5):**
   PV mounted on the roof of the charging station operates in cooperation with the BESS, as described in Section 3.3.3. The EMS coordinates BESS operation based on charging load, SoC, and electricity prices.

4. **Optimised BESS Operation (Scenario S6):**
   The battery is controlled using the rolling horizon optimiser, introduced in Section 3.4.2. The optimiser uses load, PV and price forecast to optimise the battery dispatch from the current timestep until the end of the day, while satisfying the technical constraints and providing real-time voltage support

5. **Optimised BESS Operation with Decoupled Voltage Controller (Scenario S7):**
   The optimiser is decoupled from the voltage support, only serving economical dispatch. Voltage support is provided by the reactive power output of the converter through a separate local droop controller.

Each simulation is performed using the same stochastic charging profiles, including the realistic summer PV generation profile. To evaluate the performance of the optimiser across multiple locations, configurations 1 and 5 are repeated with the charging station located at node 9, forming Scenario S8/S9.

**Multi-Station Scenarios**

To investigate the interaction between multiple HDEV charging stations and the benefits of a coordinated central voltage control, additional scenarios are constructed with multiple charging stations present.

In these scenarios, two or three identical charging stations (e.g., each with 10 charging points) are connected at different network nodes, each with a BESS and a PV system. The charging profiles of each station are independent and distinct, but are constructed using the same stochastic tool as a single charging station (Section 4.1).

Two multi-station configurations are studied:

1. **Local Voltage Control (Scenario S10):**
   Each has its own optimiser EMS for active power control and a local droop controller, mitigating voltage drop through reactive power injection.

2. **Centralised Reactive Power Dispatch (Scenario S11):**
   The reactive power set points of all stations are determined by a central controller, which minimises the total reactive power injection and smoothens the converter output, while maintaining the voltage within the predefined dead band.

3. **Varying location(Scenario S12(1/2/3/4):**
   Two charging stations, at various location. Two at the worst locations, one at the worst and one at the best location, two at the best location, and two at mediocre locations.

These scenarios highlight the difference between pure local voltage control and central coordinated reactive power support. This emphasises the improvement in voltage profiles and reactive power sharing achieved by the central controller.

**Meshed Grid Scenario**

To evaluate the performance of the mitigation strategy, a case study is conducted in a grid operation setting different from that discussed in Section 4.1. In this setting, all switches which were closed in the previously discussed scenarios will now be closed. This creates a meshed grid topology, which will show a different behaviour.

For this scenario, the following simulations will be performed:

1. **Base Line Scenario:(Scenario S13):**
   This scenario will represent the network conditions of the meshed grid without any charging station present.

2. **Unmitigated Charging (Scenario S14):**
   three charging stations will be connected at various locations in the network, one at a good location, one at a mediocre location, and one at the worst location.

3. **Mitigated Charging (Scenario S15):**
   Mitigation with an optimised control for active power and centralised reactive power dispatch will be used as a mitigation strategy.

**Overview of Scenarios**
Table 4.3 summarises all scenarios considered in this study.

**Table 4.3:** Overview of simulation scenarios.

| ID | Grid | Stations | Nodes | Charging points | Gen. seed | Mitigation | EMS control | Q control |
|---|---|---|---|---|---|---|---|---|
| S0 | Radial | 0 | – | – | – | – | – | – |
| S1 | Radial | 1 | 6 | 5 | 123 | none | – | – |
| S2 | Radial | 1 | 6 | 5 | 123 | BESS | heuristic | – |
| S3 | Radial | 1 | 6 | 10 | 123 | none | – | – |
| S4 | Radial | 1 | 6 | 10 | 123 | BESS | heuristic | – |
| S5 | Radial | 1 | 6 | 10 | 123 | PV + BESS | heuristic | – |
| S6 | Radial | 1 | 6 | 10 | 123 | PV + BESS | optimiser | – |
| S7 | Radial | 1 | 6 | 10 | 123 | PV + BESS | optimiser | local droop |
| S8 | Radial | 1 | 9 | 10 | 123 | none | – | – |
| S9 | Radial | 1 | 9 | 10 | 123 | PV + BESS | optimiser | local droop |
| S10 | Radial | 3 | 6 + 9 + 11 | 10 + 10 + 10 | 123/122/121 | PV + BESS | optimiser | local droop |
| S11 | Radial | 3 | 6 + 9 + 11 | 10 + 10 + 10 | 123/122/121 | PV + BESS | optimiser | central Q control |
| S12 | Radial | 2 | (6+6)/(1+6)/(1+1)/(2+3) | 10 + 10 | 123/121 | PV + BESS | optimiser | central Q control |
| S13 | Meshed | 0 | – | – | – | – | – | – |
| S14 | Meshed | 3 | 3 + 6 + 12 | 10 + 10 + 10 | 123/122/121 | none | – | – |
| S14 | Meshed | 3 | 3 + 6 + 12 | 10 + 10 + 10 | 123/122/121 | PV + BESS | optimiser | central Q control |

# 5

# Results and Discussion

This chapter presents the results of the simulation study, which evaluates how an MV-grid is affected by multi-megaawatt HDEV charging stations in terms of performance, stability, and efficiency. These results directly address the main research questions in this study: (1) what is the impact of high power charging on voltage profile, transformer loading and network losses, and (2) to what extent are mitigation strategies, such as BESS, PV and EMS optimisation, able to effectively reduce this impact. This chapter systematically compares baseline conditions, uncontrolled charging, and mitigation scenarios, which allows a clear evaluation of the contribution of each technology to improved grid conditions.

**Voltage Sensitivity Matrix**

In Figure 5.17 on the left, the VSM is shown for active power and on the right, the VSM is shown for reactive power. In this Figure, bus 1 is the infinite bus representing the bus connection to the transmission grid. Therefore, the numbering in the Figure is +1 with the numbering in Section 4.1. In the Figure, three buses show the highest voltage sensitivity, e.g. 6, 7, and 11. The figure also shows that, in this radial network, the voltage is more sensitive to reactive power injection or extraction. A detailed version of these matrices can be found in Appendix A.3.

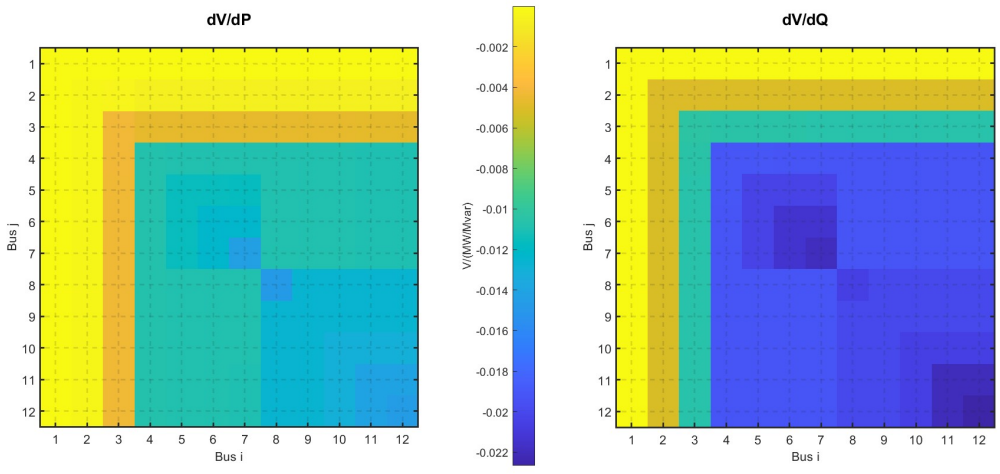


**Figure 5.1:** Voltage Sensitivity Matrix Radial Grid

## 5.1. Single Station Scenarios

This section analyses the impact of the introduction of HDEV charging stations on the baseline network. Scenario S1 includes a charging station of 5 chargers at node 6, while scenario S3 increases the number of chargers at the station to 10, both operating without any mitigation.

### 5.1.1. Single Station Impact Analysis

#### Charging Profiles

The charging profiles for both scenarios are plotted in Figure 5.2. These load profiles define the extra load in the network introduced by the charging stations. It shows that both charging profiles have approximately the same peak load. However, the overall demand of the charging station with 10 charging points is much higher, compared to 5 charging points, as the overall occupation with more charging points is higher.

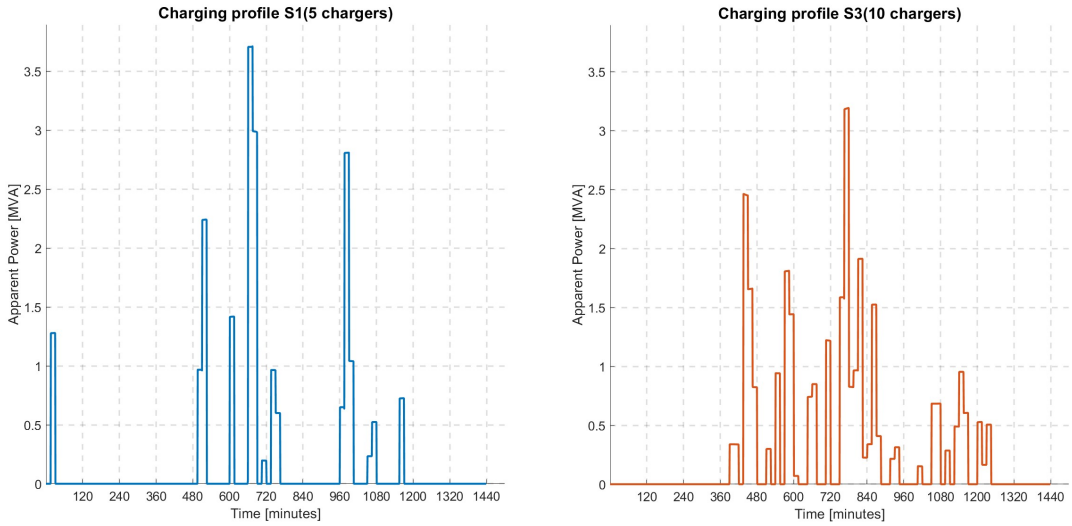


**Figure 5.2:** Charging profiles of charging station with 5/10 charging points

#### Battery sizing

**Table 5.1:** BESS power and energy rating determined from the sizing procedure.

| Charging station size | BESS power [MW] | BESS energy [MWh] |
|---|---|---|
| 5 charging points | 2.5 MW | 2.5 MWh |
| 10 charging points | 3.3 MW | 3.3 MWh |

The procedure to determine the size of the battery, described in Section 3.3.1, is applied for both a 5-point charging station and a 10-point charging station connected to bus 6. It is assumed that the BESS can deliver a maximum C-rate of 1, resulting in the BESS power rating and capacity, described in Table 5.1.

#### Voltage Profiles

Figure 5.3 shows the voltage profiles of all buses for scenarios S1 and S3, respectively. Both scenarios show severe voltage drops during charging events, with the lowest voltages occurring at node 6, where the charging station is connected. In both scenarios, the minimum voltage lies around 0.915 p.u. Even though the minimum voltage in both cases is similar, it can be observed that in scenario S3, the number of voltage dips is significantly higher compared to S1. The voltage deviation can be observed for all other nodes a well, but the magnitude of deviation from the baseline scenario is smaller for nodes located closer to the substation.

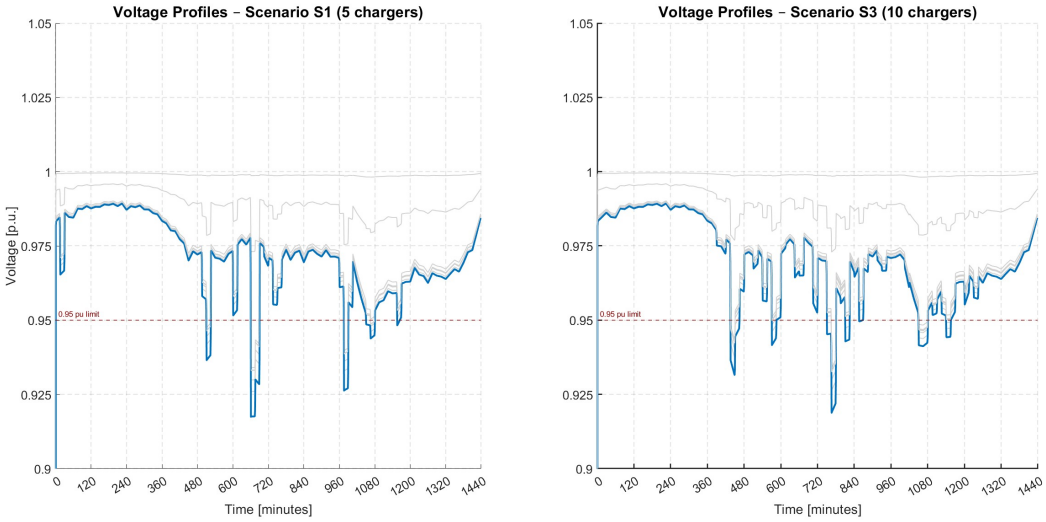


**Figure 5.3:** Bus voltages in scenario S1(Charging points) and S3(10 charging points

### Substation Power Flow

Figure 5.4 compares the loading of the substation under baseline conditions and under scenarios with 5 and 10 charging points. The main daily pattern is preserved across all scenarios. Introducing a charging station in this MV network results in only a small increase in apparent power drawn from the upstream grid. As shown, the transformer stays well below the rated capacity of 25 MVA. This shows that de impact of the charging station on transformer loading in this network is limited, and therefore not the bottleneck to be mitigated.


**Figure 5.4:** Transformer loading for for the uncontrolled scenario (S3) and with a charging station with 5/10 charging points(S1/S3)

### Line Losses

The cumulative line losses for both active and reactive power presented in Figure 5.5 show a sharp increase in line losses when a charging station of 5 charging points is introduced. This increase is even bigger in the scenario where the charging station has 10 charging points. This is in contrast with the results of the substation analysis, where only a minor increase was detected and remained well within its capacity limits. The additional current flowing through the feeder to the node furthest away from the substation has a disproportional effect on the total energy dissipation along the lines.

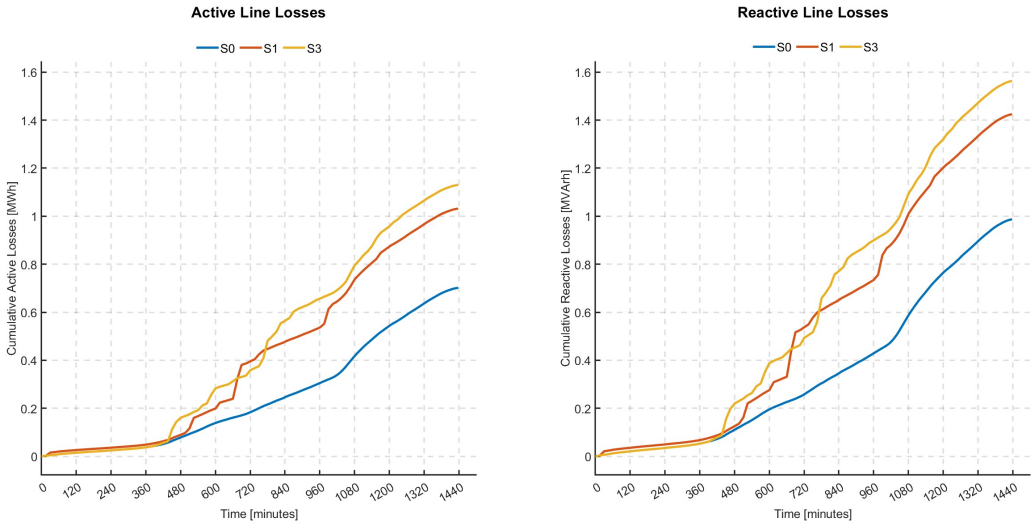


**Figure 5.5:** Losses along the power lines

### 5.1.2. Mitigation Scenarios of Single Station Charging

#### Voltage Profiles

Figures 5.6 and 5.7 show the voltage magnitude of node 6 for the uncontrolled scenario (S3) and with the three mitigation strategies (S5/S6/S7). In the morning, at around 08:00, S3 shows a dip in voltage, reaching a minimum of 0.93 p.u. With the introduction of the BESS with heuristic control, the voltage was maintained at a level around 0.95, as was the case for the other dips below the 0.95 level. Adding PV generation only had a minor effect on voltage levels, with the greatest effect concentrated around midday. Installing the optimiser-based EMS (S6/S7) has the most significant effect on the voltage. It ensured the voltage was well above 0.95 p.u. throughout the entire day. In scenario S7, where the voltage control is done by a separate droop controller, using reactive power for voltage control, the voltage has an even smoother response by levelling the voltage at the limit, without the significant use of active power.

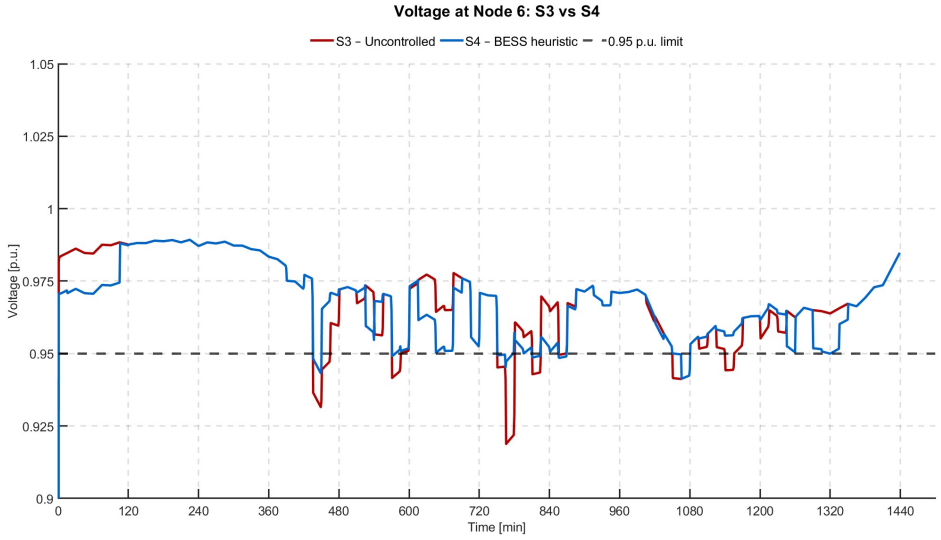


**Figure 5.6:** Voltage profile at for the uncontrolled scenario(S3) and the heuristic BESS mitigation (S4)

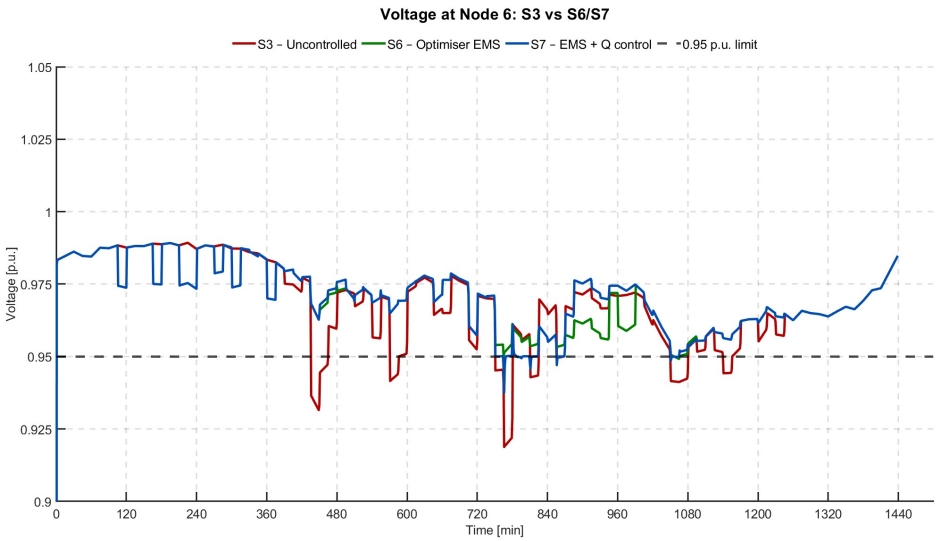


**Figure 5.7:** Voltage profile at Node 6 for the uncontrolled scenario (S3) and with BESS with optimser (and Q-control) (S6/S7)

### Distribution Transformer Loading

Figures 5.8 and 5.9 compare the distribution transformer of the charging station of the uncontrolled scenario (S3) with two mitigation scenarios(S4/S6). For both scenarios can be observed that the peak power of the station is significantly reduced. In the case of heuristic BESS control (S4), the highest peak observed at the distribution transformer is 1.9 MVA, whereas with the optimiser-based control, it is only 1.3 MW. The transformer loading in Scenario S4 shows higher and more spikes during the day. In comparison, more frequent spikes are observed in scenario S6 at night, when the BESS recharges, because it optimally charges based on electricity costs.

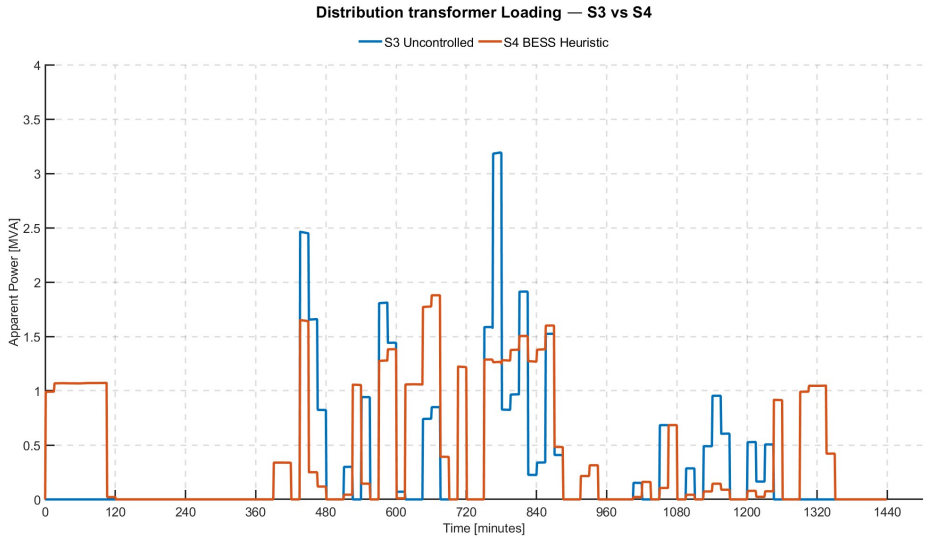


**Figure 5.8:** Distribution transformer apparent power for the uncontrolled scenario(S3) and the heuristic BESS mitigation (S4)

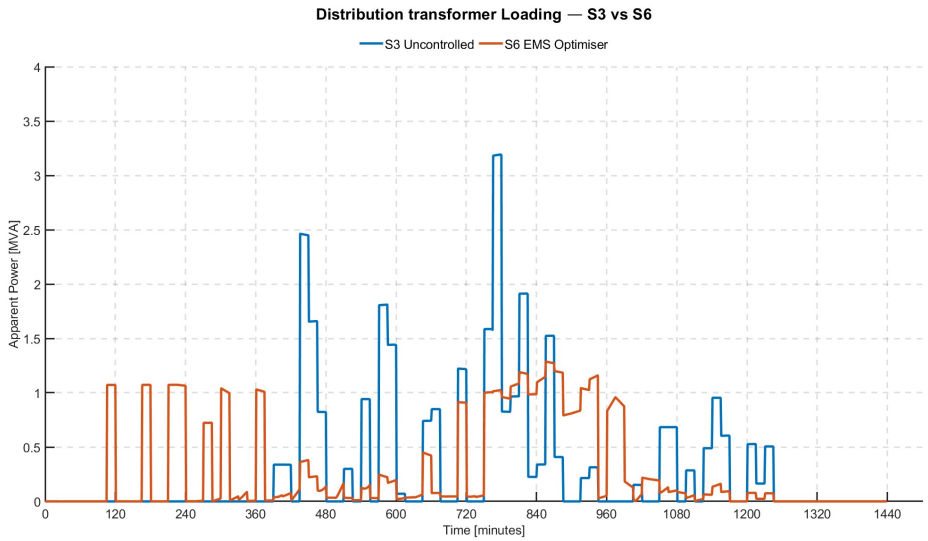


**Figure 5.9:** Distribution transformer loading for the uncontrolled scenario (S3) and with BESS with optimser (S6)

### Substation Transformer Loading

Figures 5.10 and 5.11 compare the loading of the upstream substation of the uncontrolled scenario with the two mitigation strategies concerning load reduction (S4/S6). In the uncontrolled scenario, in the morning and afternoon, charging windows show an increase in peak load, forming the dominant peaks of the day.

Introducing a BESS at the charging stations results in a reduction of this peak load in both scenarios. With the heuristic control, a slight decrease in maximum apparent power can be observed during peak moments, even though the overall shape remains similar. In the case of the optimiser-based EMS, significant smoothing of the demand from the charging station is accomplished.

Both mitigation strategies also show periods in which the load of the transformer is increased compared with the uncontrolled scenario, particularly during the night and around midday. This is expected behaviour as the BESS must also be recharged to provide peak shaving at peak periods.

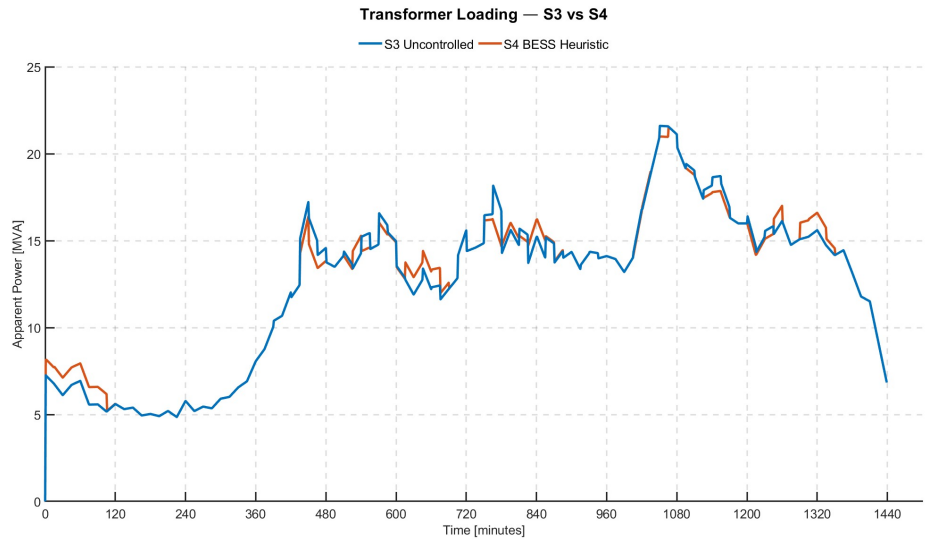


**Figure 5.10:** Substation apparent power for the uncontrolled scenario(S3) and the heuristic BESS mitigation (S4)

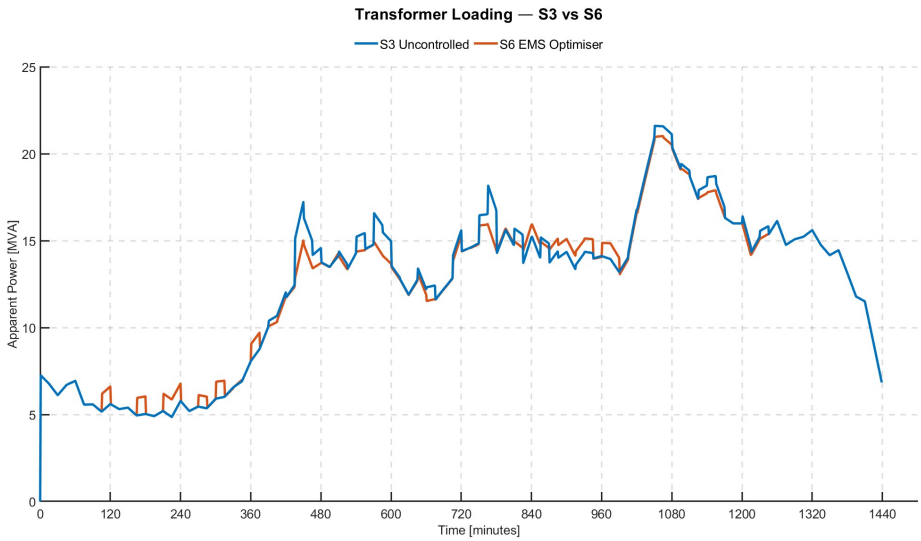


**Figure 5.11:** Substation apparent power for the uncontrolled scenario (S3) and with BESS with optimser (S6)

### Line Loading and Losses

Figure 5.12 shows the current for the main feeder line, which is the most congested line of the feeder. Figure 5.12 presents the loading of line 1-2 of the feeder, which is used to transport most of the electricity through the feeder. 5.13 shows the cumulative losses of active and reactive power along the network lines for the uncontrolled scenario (S3) and all the mitigation scenarios (S4-S7). The patterns differ due to different charging/discharging behaviours of the BESS and additional power supply by the PV system.

The heuristic-controlled BESS (S4) shows no reduction in line losses compared to the uncontrolled scenario (S3). Instead, there is a slight increase in line losses. This can be explained by the charging cycles of the BESS, which also introduces extra current in the network at moments which had otherwise low currents. This is visible in the Figure 5.12. During the afternoon hours, the line must transport more current than in the uncontrolled scenario. Because the heuristic-controlled BESS has no optimised charging schedule, the peak-shaving effects have been outweighed by the additional current, resulting in increased losses.

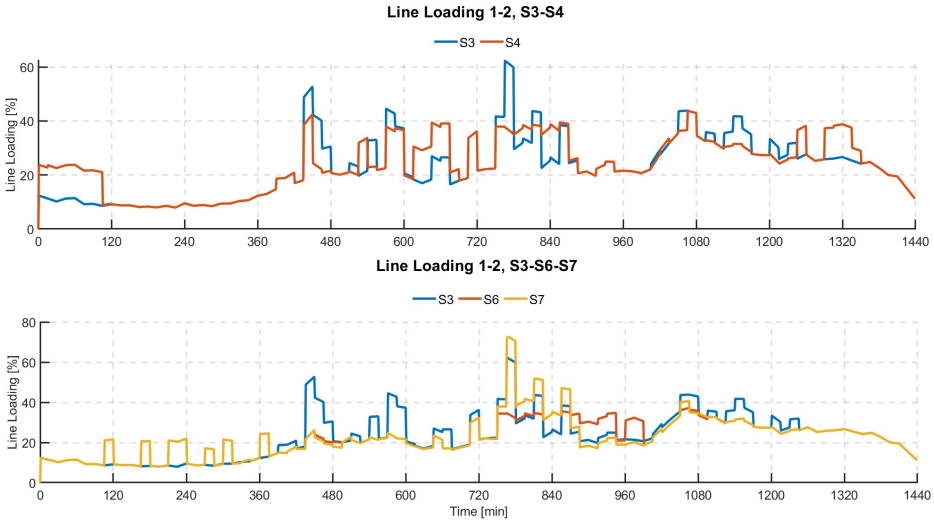


**Figure 5.12:** Line Loading of Main Feeder Line

In contrast with the heuristic controller shows the optimiser-based EMS (S6) a significant reduction in both active and reactive power losses. With an optimal active power dispatch of the BESS, currents are minimised and show a notably lower curve than the other scenarios. For active power, a reduction of approximately 18% can be observed. This shows the effectiveness of the optimiser in BESS control. Against expectation, scenario S7 has an increase in peak line loading, which is during afternoon hours, in which it is preferable to charge the BESS, during times in which the charging station is also occupied, resulting in a higher peak current.

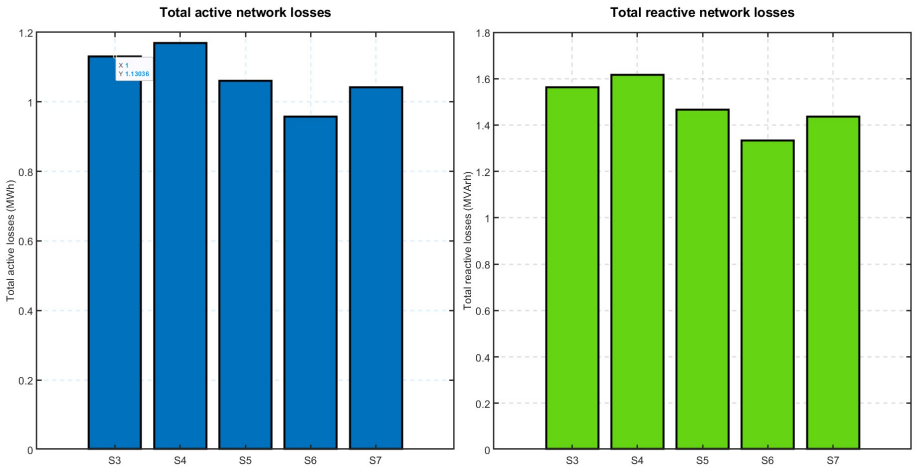


**Figure 5.13:** Line losses for the uncontrolled scenario and with all mitigation

### BESS Behaviour

The graphs in Figure 5.14 show the active power of the BESS in all the mitigation scenarios. The active power profile of the BESS with heuristic control (S4/S5) shows substantially lower BESS usage than that with optimisation control (S6/S7). In these initial scenarios, the battery is charged quickly at the start of the simulation until it reaches full SoC. During the day, it only provides active power at a limited number of time intervals. Table 5.2 shows that the net energy of the BESS has increased by more than 2 MWh for these two scenarios.

In scenarios with the optimisation control, the energy stored has increased less, whereas the throughput, especially in scenario S6 is higher. Therefore, the utilisation of the battery's full capacity is much higher. No charging occurs in the evening in these scenarios, as the battery has sufficient SoC to start a new day and a full night ahead to recharge, which cannot be accounted for in the heuristic BESS control. Therefore, different charging schedules can be observed between these control strategies. In addition, for scenario S7, it can be observed that there are fewer peaks of active power in the afternoon, as voltage support is provided by reactive power rather than active power.

**Table 5.2:** BESS throughput and peak power per scenario

| **Scenario** | $Throughput(MWh)$ | $E_{Discharge}(MWh)$ | $E_{Charge}(MWh)$ | $\Delta E_{BESS}(MWh)$ | $P_{max,dis}(MW)$ |
|---|---|---|---|---|---|
| S4 | 8.22 | 3.03 | 5.20 | 2.17 | 2.10 |
| S5 | 7.97 | 2.87 | 5.03 | 2.16 | 1.79 |
| S6 | 9.19 | 4.03 | 5.16 | 1.14 | 2.20 |
| S7 | 7.76 | 3.29 | 4.46 | 1.16 | 2.20 |

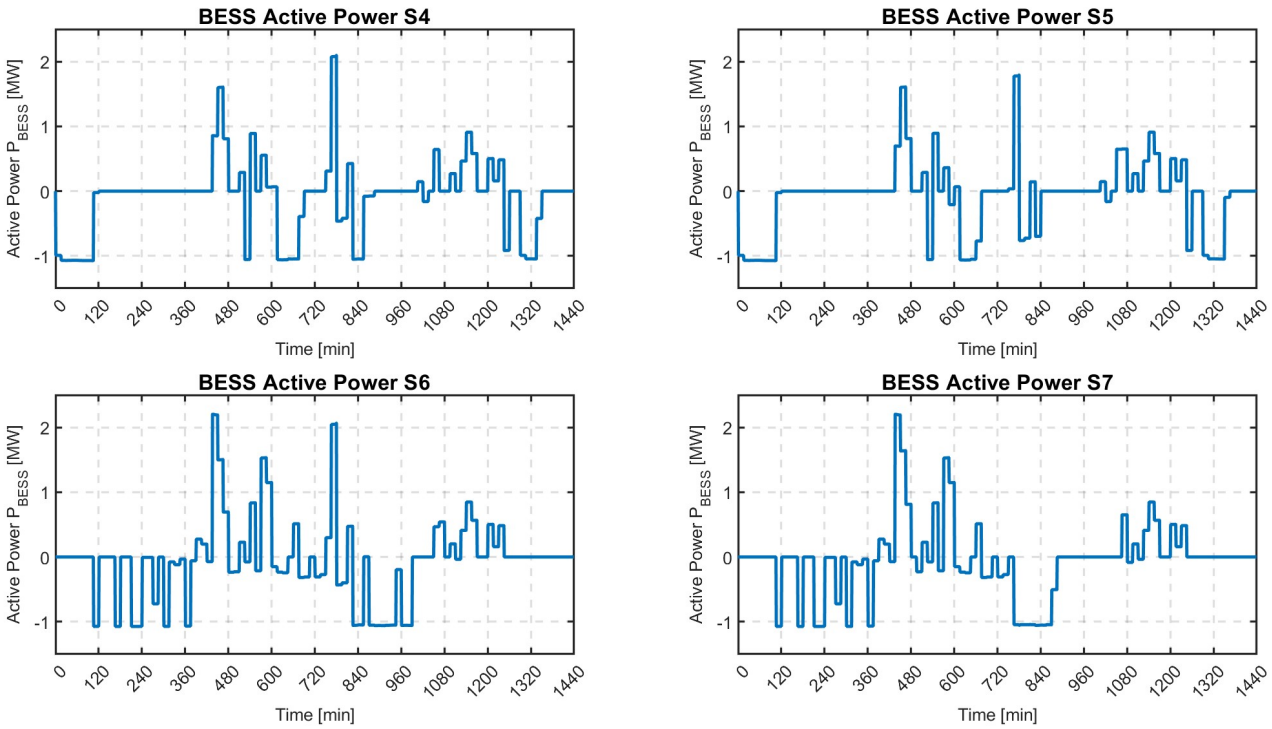


**Figure 5.14:** Active power of BESS in all mitigation scenarios (S4-S7) for a single charging station

## 5.2. Multi Station Scenarios

In this Section, multiple charging stations are added to the network to demonstrate the applicability of the control strategies in an environment with multiple EMSs present.

### 5.2.1. Triple Station Scenarios

#### Voltage Profiles

In Figure 5.15, the voltage profiles of the two critical nodes in the network are shown, for the scenarios with local Q-control and central Q-control. It shows the profiles between 12 a.m. and 6 p.m. It can be observed that when the BESS operates with only a local droop controller, oscillations occur when the voltage of critical nodes drops below the 0.95 limit. When the droop controller is driven by a central controller which actively dispatches the reactive power output of the BESSs, the voltage shows a steady and quick recovery after a voltage drop.

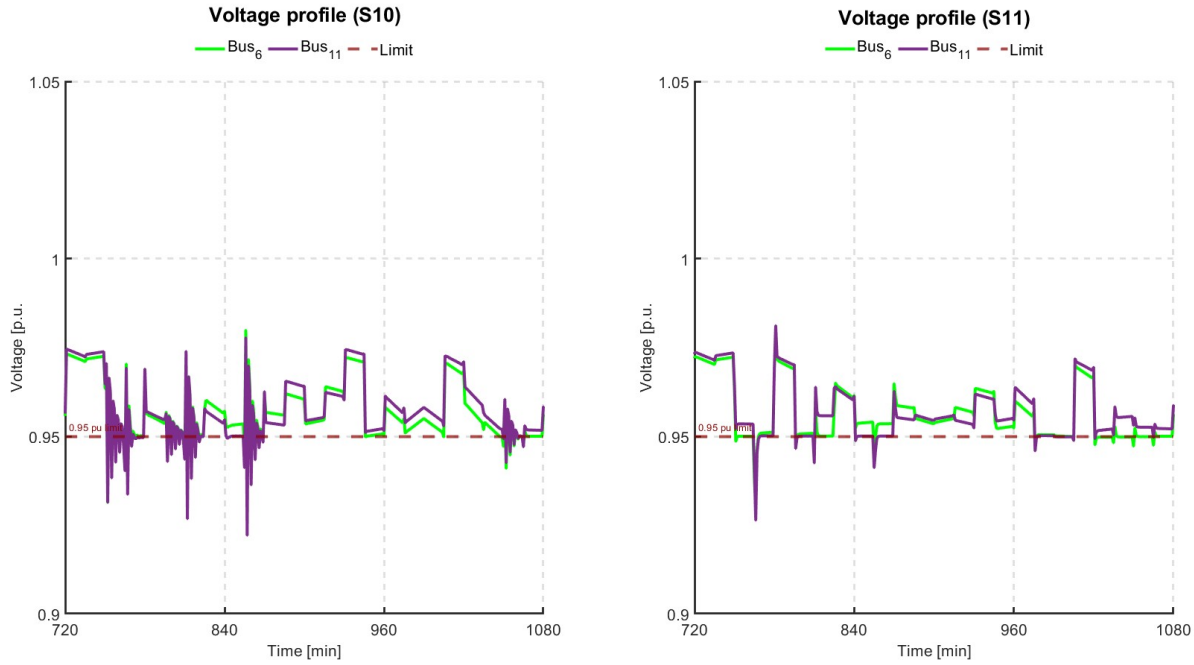


**Figure 5.15:** Voltage profile of critical nodes for scenarios with local and central Q-control (S10/S11)

### 5.2.2. Stations at Various Locations

#### Voltage Behaviour

Figure 5.16 illustrates the minimum voltage margin from the limit within the 24 hr period, for four multi-station scenarios, with each scenario having a combination of locations. On the left, the total minutes of all nodes combined in which the voltage limit is exceeded. In both the depth of the margin and the duration of the voltage limit violations, the scenario with two charging stations connected to the weakest node of the network scores the worst. It has the lowest minimal margin and the longest duration of voltage violations. On the other hand, when both charging stations are connected to the best location in the network, no nodal voltage violates the voltage limit and holds a positive minimum margin.

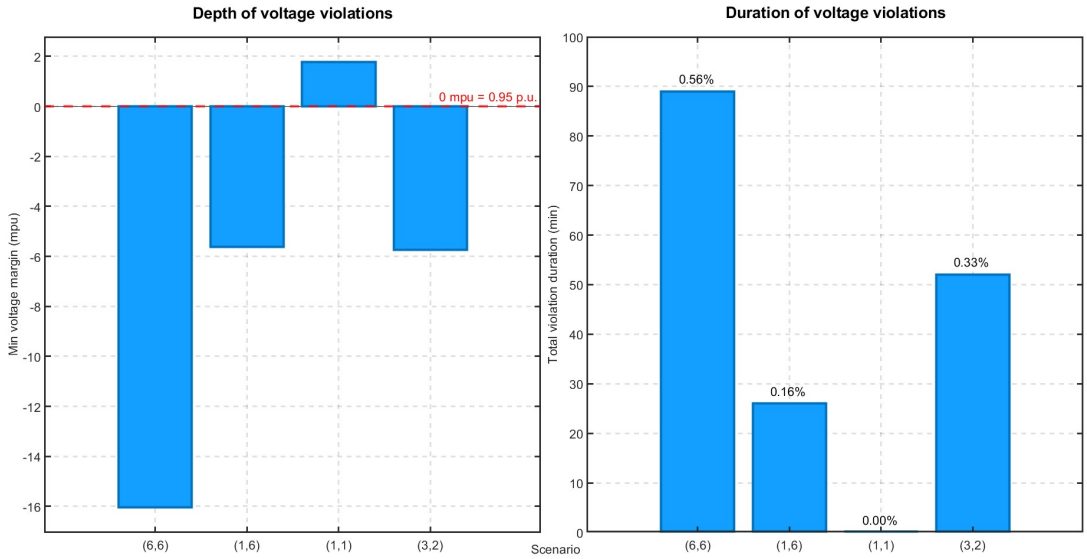


**Figure 5.16:** Voltage depth and duration of violations for varying locations (S12)

### 5.2.3. Mitigation in a Meshed Grid

#### Voltage Sensitivity Matrix

Below, the voltage sensitivity map of the meshed grid topology is shown. For the largest part of the network, the voltage sensitivity for both the active and reactive power is in the range of $6 * 10^{-3}$ p.u./(MW/MVar). As in the sensitivity map for the radial configuration, bus one in the figure acts as the slack bus, and the actual buses are Bus(i,j)-1. The Figure shows that in the meshed network, the voltage is also more susceptible to reactive power than active power. It can also be observed that in this configuration, an extra feeder is present, starting from bus 12(bus 13 in the figure). Buses 1 and 12 are connected to the substation feeder and thereby show a very low voltage sensitivity. Both node 5 and 11 show a high voltage sensitivity compared to the other nodes in the network, showcasing their vulnerability.

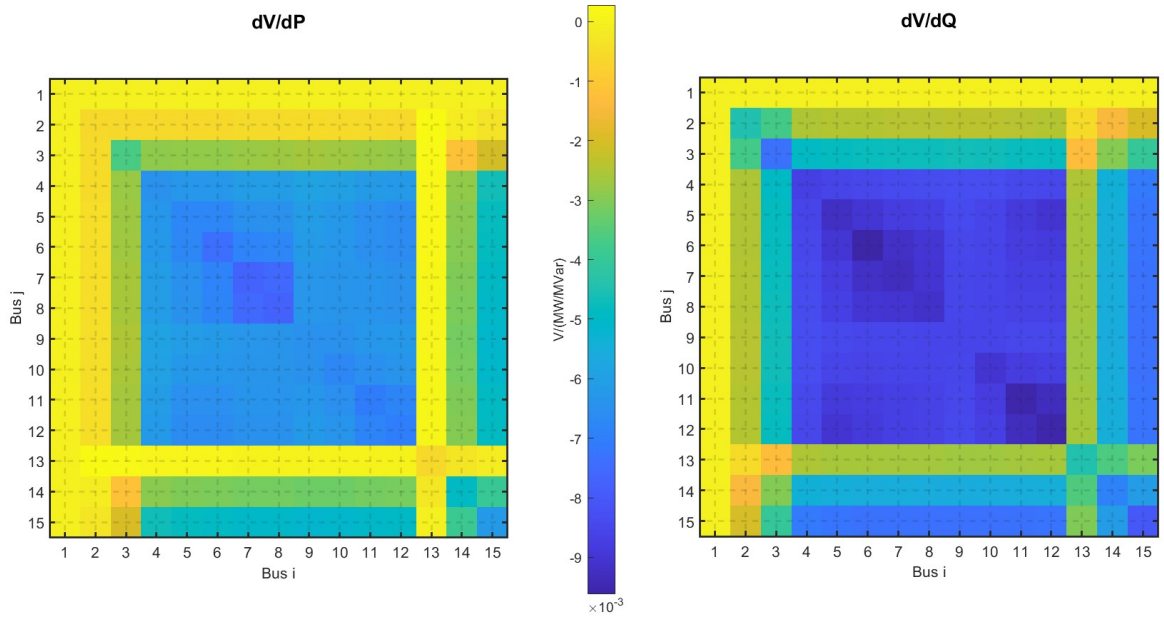


**Figure 5.17:** Voltage Sensitivity Matrix Meshed Grid

### Voltage profile and behaviour

Figure 5.18 shows the voltage profile of the weakest node of the meshed grid. Both scenarios with and without mitigation are illustrated. Without mitigation, multiple steep drops in the voltage occur, especially in the morning and afternoon. When mitigation is deployed at the charging stations, a large portion of these drops is avoided, and the voltage violations are almost eliminated. This is best illustrated in Figure 5.19, where the margin depth and duration of voltage violation over a day are given. The depth below the limit is decreased by a factor of 8 and the duration of the violations by a factor of 35.

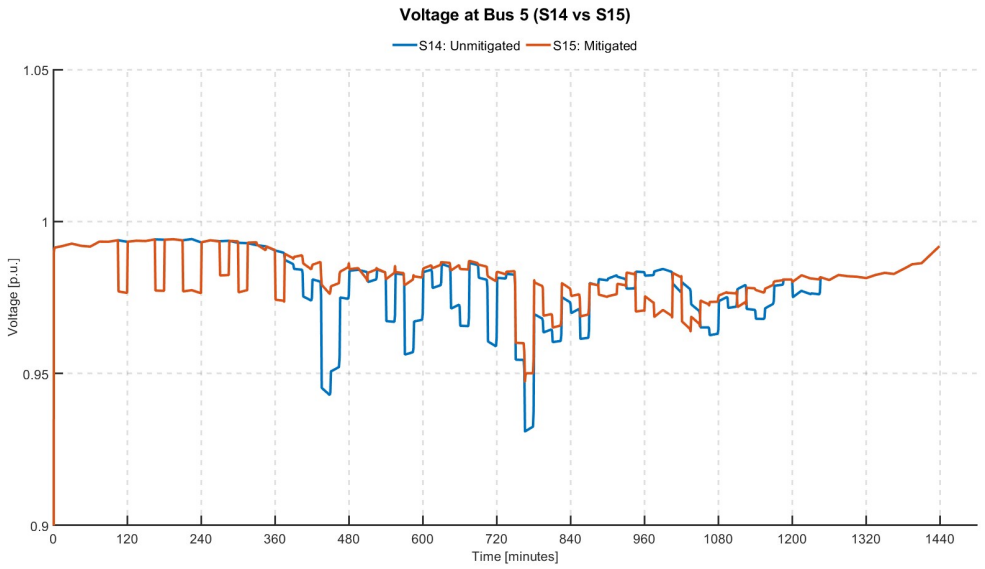


**Figure 5.18:** Voltage profile of weakest node in Meshed grid with and without mitigation (S14/S15)

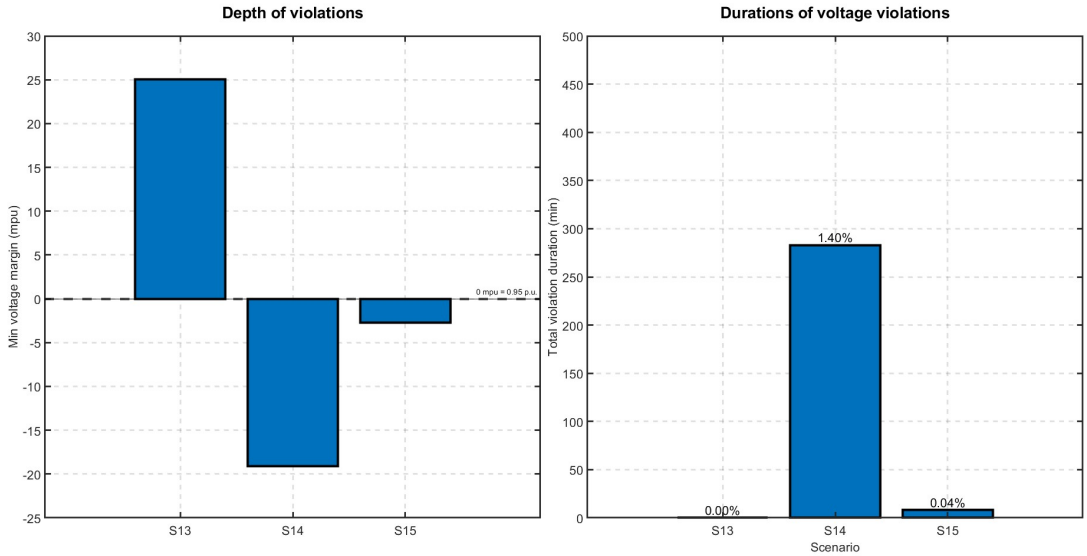


**Figure 5.19:** Voltage depth and duration of violations in a meshed grid (S13/S14/S15)

## 5.3. Discussion

This section discusses the implications of simulation results for the integration of HDEV charging stations of varying sizes into MV distribution networks, with the main focus on voltage behaviour, network loading, and the effectiveness of several BESS control strategies.

Before discussing mitigation strategies, it is essential to understand the impact of the introduction of the charging station on the distribution grid. The simulation of both with a charging station of 5 charging points and with 10 charging points imposes significant stress on the local voltage profile of the nodes in the distribution network. Voltage drops are most significant at weak nodes, particularly at a weak node near the connection point of the charging station.

Increasing the number of charging points at the charging station has been shown to amplify the depth of the voltage profiles, and at some points also their duration. When more charging points are available, the probability of clustered charging events increases, as does the likelihood of longer-duration of high loads. This leads to higher power demand of the station and higher currents drawn from the feeder. These higher currents lead to higher voltage drops due to the line impedances.

Despite the occurrence of several voltage drops, the loading of the upstream substation transformer and the local distribution transformer of the charging station remains well within their limits. This indicates that in the investigated network configuration, transformer overloading will not form a bottleneck when integrating HDEV charging stations. Instead, voltage deviation and line loading emerge in the simulations as the dominant impact factor.

The deviation in voltage observed in the first simulations and the limited utilisation of the substation transformer indicated that the impact of HDEV is predominantly a local problem. Because voltage deviations and increased currents mainly occur close to the charging station, mitigation measures targeting these local issues are expected to be more effective than upstream grid reinforcements. This supports the deployment of decentralised mitigation strategies, such as BESS and a local EMS. These measures can influence the power flow between the grid and the charging station and, thereby, indirectly affect voltage levels and line loading.

With the introduction of local mitigation with a BESS, the voltage profile of critical nodes is substantially improved across all considered mitigation scenarios. By limiting the power import from the grid during periods of high charging demand, the BESS effectively reduces voltage drops and maintains the voltage around the operational voltage. In contrast to unmitigated scenarios, voltage limit violations are almost entirely eliminated or reduced to very short periods, after which the voltage recovers. This demonstrates the ability of a BESS to address the most severe grid impacts associated with HDEV charging.

Even though the voltage profiles in all mitigation scenarios in this study are improved, the difference in control has a noticeable effect on the network conditions. These differences in control lead to specific charging-discharging patterns of the BESS. This affects the distribution transformer loading, line loading and battery utilisation. Part of this can be attributed to the control's design, which incorporates the interests of both the charging station operator and the grid operator. This approach is chosen to represent a realistic interaction between these actors in the deployment of flexible assets as BESS. In practise, the operation of these assets is shaped by both economic incentives and technical grid requirements.

The heuristic control strategy primarily mitigates voltage deviations by actively reducing the net power imported from the grid during peak demand. Thereby, voltage drops observed in the unmitigated scenarios are almost fully eliminated, and the peak power is substantially reduced. With this approach, feeder currents are reduced, resulting in smoother demand patterns at the connection point. However, due to the fact that this controller can only act on inputs of the current situation, it has reached a full SoC at the end of the day. This possibly has increased the power demand during hours when it was not desired. Charging during the night hours has less impact as the grid is less stressed during these hours.

On the other hand, the optimisation-based control has a more complex operation and interaction with the grid. Using load forecasting, the optimiser selects specific time frames for charging and maintains a sufficient SoC to provide support when needed. Charging events are shorter because the optimiser prioritises cost reduction. Although it mitigates the voltage drops with a smoother operation than the heuristic control, it does not minimise the power flows in the same way. Therefore, the cumulative line

losses show a distinct pattern, with reductions less obvious, especially when voltage support is achieved through reactive power rather than active power.

The difference in line losses reveals the trade-off between actively reducing the apparent power from the grid through active power voltage support, or through the injection of reactive power to maintain a respectable voltage level. Using active power leads to lower grid power import and lower feeder currents, but may not be cost-effective. On the other hand, using reactive power injection could lead to higher feeder currents, but could be more favourable for the charging station operator. These findings highlight the trade-off between voltage compliance, cost and network efficiency.

Extending the analysis to scenarios with multiple charging stations provides insights into the effectiveness of local mitigation strategies when deployed across multiple locations within the distribution grid. While individual charging stations primarily have a local effect at their connection point, multiple charging stations introduce a cumulative impact that affects a larger part of the distribution grid.

The results show that when voltage regulation is performed locally, the voltage in the network becomes unstable, as multiple power sources attempt to mitigate the same voltage drop. This causes oscillations in the nodal voltages when the voltage drops below the limit at certain locations in the network. These findings highlight the need for a central controller that dispatches the available reactive power at each charging station.

This central controller ensures that the voltage across the network remains within its limits. Taking into account the size of the BESS of each charging station and its voltage sensitivity at the location of the voltage violation, this approach ensures a fair and even distribution of voltage support responsibility. The simulations show a quick and smooth recovery when the central controller is applied, and the oscillations are eliminated.

Varying locations with respect to separate charging stations show how the effectiveness of this mitigation strategy is affected by the position in the distribution grid. The depth of the voltage violations shows that at every location, the BESS control preserves the voltage limit almost perfectly. Notably, the duration of voltage violations is longer when the charging stations are placed at two mediocre locations than at one worst and one best location. This can be explained by the fact that the majority of the voltage drop in the network can be attributed to the first two feeder lines. When both charging stations are placed after one of these lines, the impact on the voltage is greater than placing one station at the worst location.

The case study of the meshed grid has shown that the network behaviour, and thereby the weaknesses and strengths, change when additional interconnections are made in the network. The comparison of the mitigated and unmitigated scenarios in this network has shown a large capability of the mitigation measure to overcome voltage deviations. Voltage limit violations are almost entirely eliminated when mitigation is applied, thereby showing the effectiveness in changing grid topologies.

These findings are partly consistent with the broader literature discussed in Chapter 2, in which a strong emphasis is placed on the impact of HDEV chargers on local voltages. This study showed that voltages, even at a charging station with only 5 charging points, exhibit significant deviations outside the allowable limits. Studies of [18] and [19] showed the same level of peak load reduction with the introduction of a BESS. That substation transformer loading levels were not the bottleneck in the simulation aligns with the findings of [12], which indicate that the real bottleneck was line loading rather than transformer loading. In the single-station scenarios, line overloading still hasn't been reached, but when more charging stations are added to the network, lines start to get congested.

However, the results of this study extend the body of literature on HDEV charging and demonstrate a clear difference in the operation of heuristic and optimisation-based control strategies, which have been underexplored to date. By comparing them under identical network conditions and locations, this study has demonstrated the strengths and flaws of both strategies. Centralised voltage regulation has been explored and has demonstrated its benefits in multi-station scenarios. Although reactive power for voltage control requires higher feeder currents than active power control, it offers greater integration potential with a central coordination of local voltage controlling assets, as it uses only the available spare reactive power without compromising the economical operation of the charging station operator.

# 6

# Conclusion

This thesis investigated the impact of the HDEV charging station in two MV distribution network configurations and evaluated the effectiveness of local mitigation strategies, primarily based on BESS. Due to the high charging power, clustered charging events and unpredictable charging patterns have a significant impact on these charging stations' local grid conditions, such as voltage levels and transformer loading. This study aimed to provide new insights into the effective impact mitigation for a successful integration of the HDEV charging station. This is achieved by providing a comparative analysis of multiple mitigation and control strategies, and evaluating them under distinct grid conditions and varying sizes and numbers of charging stations.

Simulation of unmitigated HDEV charging shows impacts on local grid conditions, such as voltage deviations at weak nodes and increased line loading, whereas in the investigated MV network, upstream transformer loading is not identified as a bottleneck. Using BESS-based mitigation, voltage stability is effectively restored, and the charging station's peak load is reduced. Heuristic control achieves robust peak load reduction through active power limitation, whereas optimisation-based control shows better economic effectiveness and the best performance in voltage regulation and peak load reduction. Central voltage control is necessary for steady voltage regulation when multiple charging stations with each their own local EMS are integrated into a network. A meshed topology for the MV network demonstrates the applicability of the investigated mitigation strategies.

The results of this study extend the existing literature by explicitly focusing on multi-megawatt HDEV and by comparing different control strategies. In contrast with most existing studies, the interaction between multiple charging stations, clustered charging events, and the role of central coordination for local voltage support provides new insights into the trade-offs in voltage compliance, network stability and BESS operation.

In future work, the integration of BESS degradation models could provide additional insights into the long-term ageing of assets, which was outside the scope of this study. Additionally, further research could extend the results of this study by conducting a reliability assessment, such as component failure analysis, to evaluate the robustness of mitigation strategies under faulted network conditions. Also, the use of more stochastic-like charging demand patterns would further improve the insights into the real-world implementation of such a charging station, as a limitation of this study is that it made use of pre-generated demand patterns, even though these originated from a stochastic-based model.

# Bibliography


[1] International Energy Agency. *Global EV Outlook 2025 – Trends in Heavy-Duty Electric Vehicles*. 2025.

[2] Xiangqi Zhu, Barry Mather, and Partha Mishra. "Grid impact analysis of heavy-duty electric vehicle charging stations". In: *2020 IEEE Power & Energy Society Innovative Smart Grid Technologies Conference (ISGT)* (Feb. 2020).

[3] Charging Interface Initiative (CharIN). *Megawatt Charging System (MCS)*. 2024. URL: https://www.charin.global/technology/knowledge-base/.

[4] Heikki Liimatainen, Oscar van Vliet, and David Aplyn. "The potential of electric trucks – An international commodity-level analysis". en. In: *Appl. Energy* 236 (Feb. 2019), pp. 804–814.

[5] Moufid Ismail et al. "Power losses minimization in distribution system using soft open point". In: *2020 1st International Conference on Innovative Research in Applied Science, Engineering and Technology (IRASET)* (Apr. 2020).

[6] Kyrre Kirkbakk Fjær et al. "Heavy-duty electric vehicle charging profile generation method for grid impact analysis". In: *2021 International Conference on Smart Energy Systems and Technologies (SEST)*. 2021, pp. 1–6. DOI: 10.1109/SEST50973.2021.9543135.

[7] Asiri Tayri and Xiandong Ma. "Grid impacts of electric vehicle charging: A review of challenges and mitigation strategies". en. In: *Energies* 18.14 (July 2025), p. 3807.

[8] Ali Hassan et al. "Impact of medium and heavy-duty electric vehicle electrification on distribution system stability". In: *2025 IEEE/AIAA Transportation Electrification Conference and Electric Aircraft Technologies Symposium (ITEC+EATS)* (June 2025), pp. 1–3.

[9] Joshua Then, Ashish P. Agalgaonkar, and Kashem M. Muttaqi. "Planning for Medium- and Heavy-Duty Electric Vehicle Charging Infrastructure in Distribution Networks to Support Long-Range Electric Trucks". In: *Energies* 18.4 (2025). ISSN: 1996-1073. URL: https://www.mdpi.com/1996-1073/18/4/785.

[10] Pravakar Pradhan et al. "Reducing the impacts of electric vehicle charging on power distribution transformers". In: *IEEE Access* 8 (2020), pp. 210183–210193.

[11] Matthew J Rutherford and Vahid Yousefzadeh. "The impact of Electric Vehicle battery charging on distribution transformers". In: *IEEE Access* (Mar. 2011).

[12] Thomas Oberliessen et al. "Simulation-based analysis of grid impact from large-scale HDEV charging infrastructure". In: *Institute of Electrical and Electronics Engineers (IEEE)* (May 2025), pp. 99–103.

[13] Ehsan Reihani et al. "Energy management at the distribution grid using a Battery Energy Storage System (BESS)". en. In: *Int. J. Electr. Power Energy Syst.* 77 (May 2016), pp. 337–344.

[14] Ehsan Reihani et al. "Load peak shaving and power smoothing of a distribution grid with high renewable energy penetration". en. In: *Renew. Energy* 86 (Feb. 2016), pp. 1372–1379.

[15] Grazia Barchi, Marco Pierro, and David Moser. "Predictive energy control strategy for peak shaving and shifting using BESS and PV generation applied to the retail sector". en. In: *Electronics (Basel)* 8.5 (May 2019), p. 526.

[16] Jonatan Ralf Axel Klemets, Eirik Haugen, and Bendik Nybakk Torsæter. "MPC-based control structure for high-power charging stations capable of providing ancillary services". en. In: *Int. J. Electr. Power Energy Syst.* 159.110039 (Aug. 2024), p. 110039.

[17] Ujjwal Datta, Akhtar Kalam, and Juan Shi. "Smart control of BESS in PV integrated EV charging station for reducing transformer overloading and providing battery-to-grid service". en. In: *J. Energy Storage* 28.101224 (Apr. 2020), p. 101224.

[18] Sayed Mir Shah Danish et al. "A coherent strategy for peak load shaving using energy storage systems". en. In: *J. Energy Storage* 32.101823 (Dec. 2020), p. 101823.

[19] Daniel Kucevic et al. "Reducing grid peak load through the coordinated control of battery energy storage systems located at electric vehicle charging parks". en. In: *Appl. Energy* 295.116936 (Aug. 2021), p. 116936.

[20] Xiangqi Zhu et al. "Grid impact analysis and mitigation of en-route charging stations for heavy-duty electric vehicles". In: *IEEE Open J. Power Energy* 10 (2023), pp. 141–150.

[21] Xiangjun Li, Dong Hui, and Xiaokang Lai. "Battery energy storage station (BESS)-based smoothing control of photovoltaic (PV) and wind power generation fluctuations". In: *IEEE Trans. Sustain. Energy* 4.2 (Apr. 2013), pp. 464–473.

[22] Lu Wang et al. "Grid impact of electric vehicle fast charging stations: Trends, standards, issues and mitigation measures - an overview". In: *IEEE Open J. Power Electron.* 2 (2021), pp. 56–74.

[23] Sameer Ahmed Khan Mojlish, Danny Sutanto, and Kashem M. Muttaqi. "Impacts of ultra-fast charging of electric vehicles on power grids: State-of-the-art technologies, case studies, and a proposed improvement using a solid-state transformer". In: *Journal of Energy Storage* 107 (2025), p. 114913. ISSN: 2352-152X. DOI: https://doi.org/10.1016/j.est.2024.114913. URL: https://www.sciencedirect.com/science/article/pii/S2352152X24044992.

[24] M A van den Berg, I Lampropoulos, and T A AlSkaif. "Impact of electric vehicles charging demand on distribution transformers in an office area and determination of flexibility potential". en. In: *Sustain. Energy Grids Netw.* 26.100452 (June 2021), p. 100452.

[25] Elaad. *Logistics — platform.elaad.io*. https://platform.elaad.io/chargingprofiles/. [Accessed 10-05-2025].

[26] Xiangqi Zhu et al. "A hierarchical VLSM-based demand response strategy for coordinative voltage control between transmission and distribution systems". In: *IEEE Trans. Smart Grid* 10.5 (Sept. 2019), pp. 4838–4847.

[27] Wouter Knap. "Basic and other measurements of radiation at station Cabauw (2024-07)". In: PANGAEA, 2024. DOI: 10.1594/PANGAEA.973258. URL: https://doi.org/10.1594/PANGAEA.973258.

[28] Charging Interface Initiative (CharIN). *White Paper of Charging Interface Initiative e.V*. 2025. URL: %7Bhttps://www.charin.global/technology/knowledge-base/%7D.

[29] CIGRÉ Task Force C6.04.02. *Benchmark Systems for Network Integration of Renewable and Distributed Energy Resources*. Tech. rep. CIGRÉ Report TB 575. CIGRÉ, 2014. URL: https://e-cigre.org/publication/575-benchmark-systems-for-network-integration-of-renewable-and-distributed-energy-resources.

[30] Liander. *Open data | Liander liander.nl*. [Accessed 08-05-2025]. 2025. URL: %5Curl%7Bhttps://www.liander.nl/over-ons/open-data#verbruiksdata-slimme-meter%7D.

# A

# Appendix A: Simulation Parameters

## A.1. Nodal load data

**Table A.1:** Nodal apparent power and power factor data for the CIGRE benchmark network.

| Node | Apparent Power $S$ [kVA] | | Power Factor $pf$ | |
|---|---|---|---|---|
| | Residential | Commercial / Industrial | Residential | Commercial / Industrial |
| 1 | 15 300 | 5100 | 0.98 | 0.95 |
| 2 | – | – | – | – |
| 3 | 285 | 265 | 0.97 | 0.85 |
| 4 | 445 | – | 0.97 | – |
| 5 | 750 | – | 0.97 | – |
| 6 | 565 | – | 0.97 | – |
| 7 | – | 90 | – | 0.85 |
| 8 | 605 | – | 0.97 | – |
| 9 | – | 675 | – | 0.85 |
| 10 | 490 | 80 | 0.97 | 0.85 |
| 11 | 340 | – | 0.97 | – |
| 12 | 15 300 | 5280 | 0.98 | 0.95 |
| 13 | – | 40 | – | 0.85 |
| 14 | 215 | 390 | 0.97 | 0.85 |

## A.2. Aggregated charging profile

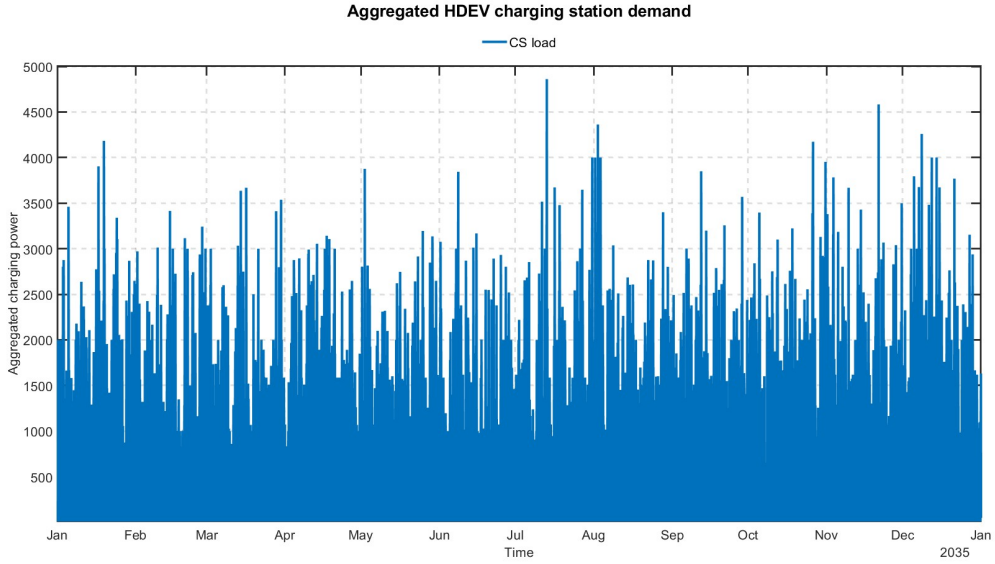


**Figure A.1**

## A.3. Sensitivity matrices

| | 1 | 2 | 3 | 4 | 5 | 6 | 7 | 8 | 9 | 10 | 11 |
|---|---|---|---|---|---|---|---|---|---|---|---|
| 1 | -0.00032 | -0.00044 | -0.00063 | -0.00064 | -0.00064 | -0.00065 | -0.00064 | -0.00064 | -0.00064 | -0.00065 | -0.00065 |
| 2 | -0.00032 | -0.00417 | -0.00464 | -0.00466 | -0.00468 | -0.00469 | -0.00468 | -0.00468 | -0.00469 | -0.00471 | -0.00471 |
| 3 | -0.00033 | -0.00425 | -0.01076 | -0.01080 | -0.01084 | -0.01085 | -0.01084 | -0.01083 | -0.01086 | -0.01089 | -0.01089 |
| 4 | -0.00033 | -0.00425 | -0.01077 | -0.01155 | -0.01158 | -0.01160 | -0.01085 | -0.01084 | -0.01087 | -0.01090 | -0.01090 |
| 5 | -0.00033 | -0.00425 | -0.01077 | -0.01156 | -0.01233 | -0.01235 | -0.01085 | -0.01085 | -0.01087 | -0.01090 | -0.01091 |
| 6 | -0.00033 | -0.00426 | -0.01078 | -0.01156 | -0.01233 | -0.01438 | -0.01086 | -0.01085 | -0.01088 | -0.01091 | -0.01091 |
| 7 | -0.00033 | -0.00426 | -0.01079 | -0.01083 | -0.01086 | -0.01088 | -0.01478 | -0.01258 | -0.01260 | -0.01264 | -0.01264 |
| 8 | -0.00033 | -0.00426 | -0.01078 | -0.01083 | -0.01086 | -0.01088 | -0.01258 | -0.01257 | -0.01260 | -0.01263 | -0.01264 |
| 9 | -0.00033 | -0.00426 | -0.01079 | -0.01083 | -0.01087 | -0.01088 | -0.01258 | -0.01258 | -0.01303 | -0.01306 | -0.01307 |
| 10 | -0.00033 | -0.00426 | -0.01080 | -0.01084 | -0.01087 | -0.01089 | -0.01259 | -0.01259 | -0.01304 | -0.01409 | -0.01409 |
| 11 | -0.00033 | -0.00426 | -0.01080 | -0.01084 | -0.01087 | -0.01089 | -0.01259 | -0.01259 | -0.01304 | -0.01409 | -0.01453 |

**Table A.2:** Sensitivity Matrix $\frac{\delta V}{\delta P}$

| | 1 | 2 | 3 | 4 | 5 | 6 | 7 | 8 | 9 | 10 | 11 |
|---|---|---|---|---|---|---|---|---|---|---|---|
| 1 | -0.00498 | -0.00503 | -0.00511 | -0.00511 | -0.00512 | -0.00512 | -0.00512 | -0.00512 | -0.00512 | -0.00512 | -0.00512 |
| 2 | -0.00505 | -0.01032 | -0.01052 | -0.01052 | -0.01053 | -0.01053 | -0.01054 | -0.01053 | -0.01054 | -0.01055 | -0.01055 |
| 3 | -0.00515 | -0.01053 | -0.01909 | -0.01911 | -0.01912 | -0.01913 | -0.01914 | -0.01913 | -0.01914 | -0.01916 | -0.01916 |
| 4 | -0.00515 | -0.01053 | -0.01911 | -0.02027 | -0.02028 | -0.02029 | -0.01915 | -0.01914 | -0.01916 | -0.01917 | -0.01917 |
| 5 | -0.00515 | -0.01054 | -0.01912 | -0.02028 | -0.02135 | -0.02135 | -0.01916 | -0.01915 | -0.01917 | -0.01918 | -0.01918 |
| 6 | -0.00516 | -0.01055 | -0.01913 | -0.02029 | -0.02136 | -0.02191 | -0.01917 | -0.01916 | -0.01918 | -0.01919 | -0.01919 |
| 7 | -0.00516 | -0.01055 | -0.01914 | -0.01915 | -0.01917 | -0.01917 | -0.02058 | -0.01997 | -0.01998 | -0.02000 | -0.02000 |
| 8 | -0.00516 | -0.01055 | -0.01914 | -0.01915 | -0.01916 | -0.01917 | -0.01997 | -0.01997 | -0.01998 | -0.02000 | -0.02000 |
| 9 | -0.00516 | -0.01056 | -0.01915 | -0.01916 | -0.01917 | -0.01918 | -0.01999 | -0.01998 | -0.02056 | -0.02057 | -0.02057 |
| 10 | -0.00516 | -0.01056 | -0.01916 | -0.01917 | -0.01918 | -0.01919 | -0.01999 | -0.01999 | -0.02057 | -0.02203 | -0.02204 |
| 11 | -0.00516 | -0.01056 | -0.01916 | -0.01918 | -0.01919 | -0.01919 | -0.02000 | -0.01999 | -0.02057 | -0.02203 | -0.02266 |

**Table A.3:** Sensitivity Matrix $\frac{\delta V}{\delta Q}$

## A.4. PV power profiles winter and summer

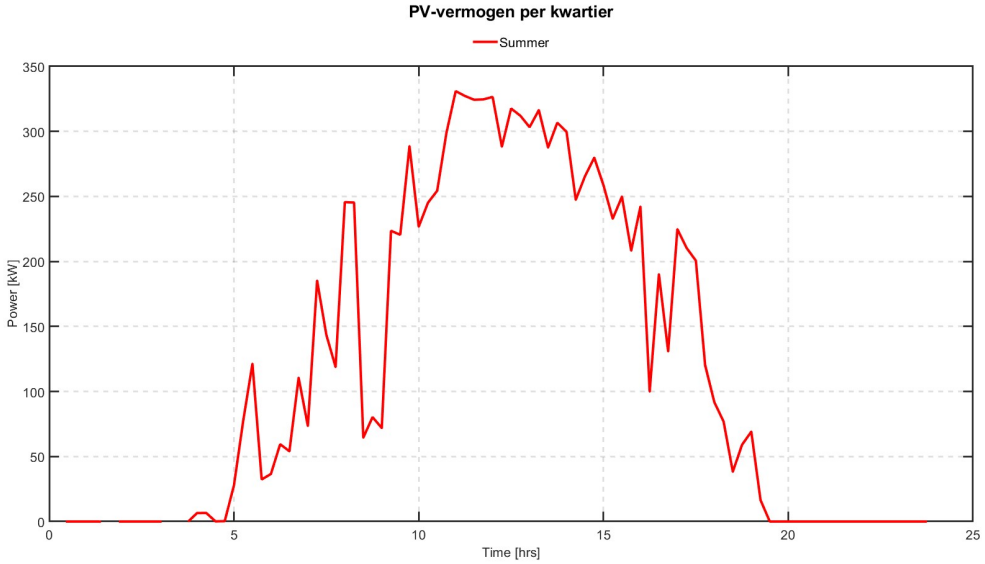


**Figure A.2:** PV system power profiles summer

# B

# Appendix B: MATLAB/Simulink Code

## B.1. Load profile generation

```
Pres_1 = loadProfile.Normalised_residential *Res_1*1000;%Apparent residential load profile
Pin_1 = loadProfile.Normalised_industrial*In_1*1000;    %Apperent industrial load profile
V_ll = 20000;                                           %line-to-line voltage
Ires = (sqrt(2) * Pres_1/ (sqrt(3) * V_ll ));           %Current residential profile
Iin =  + sqrt(2) * Pin_1/ (sqrt(3) * V_ll) ;            %Current industrial profile
Ires1_profile = [timeInSeconds, Ires_peak];             %Current residential timeseries
Iin1_profile = [timeInSeconds, Iin_peak];               %Current industriral timeseries
```

## B.2. BESS logic

### B.2.1. Heuristic controller

```
function P_batt = battery_step_interface( ...
    P_load, V_meas, price_current, SOC_current, ...
    price_vec, P_batt_prev, params, Ppv)
%#codegen
% Interface function for calling the single-step Gurobi optimizer
% from a Simulink MATLAB Function block.
%
% Inputs:
%   P_load         - current load (kW)
%   V_meas         - measured voltage (pu)
%   price_current  - current electricity price (   /kWh)
%   SOC_current    - current state of charge (0..1)
%   price_vec      - daily price vector (96x1)
%   P_batt_prev    - previous battery power (kW)
%   params         - battery parameter struct
%   Ppv            - current PV production (kW)
%
% Output:
%   P_batt         - optimized battery power (kW)

%% Declare the external (non-codegen) solver
coder.extrinsic('battery_gurobi_wrapper');

%% Initialize output
P_batt = 0;

%% Call the extrinsic Gurobi wrapper
P_batt_result = battery_gurobi_wrapper( ...
    P_load, V_meas, price_current, SOC_current, ...
    price_vec, P_batt_prev, params, Ppv);

%% Validate and assign the result
if isnumeric(P_batt_result)
    P_batt = P_batt_result;
end
```

```

end
```

```
function P_batt = battery_gurobi_wrapper( ...
Pload, Vbase, price_current, SOC_current, ...
    price_vec, P_batt_prev, params, Ppv)
% Single-step Gurobi optimizer (called externally from Simulink)
%
% Inputs:
%   Pload         - current load (kW, scalar)
%   Vbase         - measured voltage (pu)
%   price_current - current electricity price (   /kWh)
%   SOC_current   - current state of charge (0..1)
%   price_vec     - daily price vector (96x1)
%   P_batt_prev   - previous battery power (kW)
%   params        - struct containing:
%                   .C, .eta_ch, .eta_dis, .Pch_max, .Pdis_max,
%                   .SOCmin, .SOCmax, .c_deg, .S_sen, .dt
%   Ppv           - current PV production (unused but kept for interface)
%
% Output:
%   P_batt        - optimal battery power (kW)

%% 1. Parameters
dt        = params.dt;
C         = params.C;
eta_ch    = params.eta_ch;
eta_dis   = params.eta_dis;
Pch_max   = params.Pch_max;
Pdis_max  = params.Pmax;
SOCmin    = params.SOCmin;
SOCmax    = params.SOCmax;
c_deg     = params.c_deg;
S_sen     = params.S_sen;

%% 2. Price deviation factor
price_mean   = mean(price_vec(:));
price_factor = price_current - price_mean;
% Negative     cheaper than average     charging attractive
% Positive     expensive     discharging attractive

%% 3. Objective function coefficient
f = -price_factor * dt;

%% 4. SOC-based bounds
ub_SOC = (SOC_current - SOCmin) * C / dt * eta_dis;
ub_SOC = max(0, min(ub_SOC, Pdis_max));

lb_SOC = -(SOCmax - SOC_current) * C / dt / eta_ch;
lb_SOC = min(0, max(lb_SOC, -Pch_max));

%% 5. Voltage constraint including previous battery action
% V_next = Vbase + (P_batt - P_batt_prev)/S_sen >= 0.95
v_lb = S_sen * (0.95 - Vbase) + P_batt_prev;

%% 6. Max discharge cannot exceed load
ub_load = Pload - Ppv;

%% 7. Combine all bounds
lb = max([lb_SOC, v_lb, -Pch_max]);
ub = min([ub_SOC, ub_load, Pdis_max]);

% If bounds inconsistent     clamp to upper bound
if lb > ub
    P_batt = ub;
    return;
end

%% 8. Build Gurobi model
model.modelsense = 'min';
model.obj        = f;        % 1x1 numeric array
```

```
model.lb         = lb;
model.ub         = ub;
model.A          = sparse(0,1);
model.rhs        = [];
model.sense      = '';

paramsGurobi.OutputFlag = 0;

%% 9. Call Gurobi solver
try
    result = gurobi(model, paramsGurobi);
    if isfield(result, 'x') && ~isempty(result.x)
        P_batt = result.x(1);
    else
        P_batt = 0;
    end
catch ME
    warning('Gurobi solver failed: %s', ME.message);
    P_batt = 0;
end

%% 10. Safety checks
P_batt = min(P_batt, Pload);
P_batt = max(-Pch_max, min(P_batt, Pdis_max));

end
```

### B.2.2. Rolling Horizon controller

```
function P_batt = battery_controller( ...
    Pload_current, Vbase, SOC_current, t, ...
    Pload_forecast, price_vec, P_batt_prev, params, ...
    P_pv_current, P_pv_forecast)
%#codegen
% MATLAB Function block wrapper for horizon-based Gurobi solver
%
% Inputs:
%   Pload_current   : current load (scalar)
%   Vbase           : current voltage (scalar)
%   SOC_current     : current SOC (0..1)
%   t               : current timestep index
%   Pload_forecast  : forecasted load over the day (Nx1)
%   price_vec       : price vector over the day (Nx1)
%   P_batt_prev     : previous battery power (kW)
%   params          : struct containing battery parameters
%   P_pv_current    : current PV power (kW)
%   P_pv_forecast   : forecasted PV power (Nx1)
%
% Output:
%   P_batt          : active battery power for the current step (kW)

%% --- Initialization
P_batt = 0;

% Gurobi can only run in MATLAB (not codegen), so declare as extrinsic
coder.extrinsic('battery_gurobi_step_horizon_6');

% Startup behavior
if t < 1
    P_batt_prev = 0;
end

%% --- Call horizon-based solver (extrinsic)
Pbatt_tmp = battery_gurobi_step_horizon_6( ...
    Pload_current, Vbase, SOC_current, t, ...
    Pload_forecast, price_vec, P_batt_prev, params, ...
    P_pv_current, P_pv_forecast);

%% --- Validate and apply result
if isnumeric(Pbatt_tmp)
```

```
    P_batt = Pbatt_tmp;
end

end
```

```
function P_batt = battery_gurobi_step_horizon_6( ...
    Pload_current, Vbase, SOC_current, t, ...
    Pload_forecast, price_vec, P_batt_prev, params, ...
    P_pv_current, P_pv_forecast)
% Rolling-horizon Gurobi optimizer for battery dispatch
% ------------------------------------------------------
% Horizon: from current time index t to end of day.
% Only the first-step optimal action P_batt is returned.
%
% Inputs:
%   Pload_current   - actual load at current time (kW)
%   Vbase           - measured voltage (pu)
%   SOC_current     - current state of charge (0..1)
%   t               - current time index
%   Pload_forecast  - forecasted load vector (Nx1)
%   price_vec       - price vector (Nx1)
%   P_batt_prev     - previous battery power (kW)
%   params          - struct with:
%                       .dt, .C, .eta_ch, .eta_dis
%                       .Pch_max, .Pdis_max, .SOCmin, .SOCmax
%                       .SOCinit, .c_SOC, .S_sen
%   P_pv_current    - current PV power
%   P_pv_forecast   - PV forecast vector
%
% Output:
%   P_batt          - first-step optimal battery power (kW)

%% Convert internal time resolution (4 seconds     one 15 minute timestep )
t = ceil(t/4);

%% Horizon setup
N = length(price_vec);
H = N - t + 1;
dt = params.dt;

if H == 0
    P_batt = 0;
    return;
end

price_h = price_vec(t:end);

Pload_h = Pload_forecast(t:end);
Pload_h(1) = Pload_current;

Ppv_h = P_pv_forecast(t:end);
Ppv_h(1) = P_pv_current;

%% Decision variable indices
% Variables: [Pch; Pdis; SOC; Pgrid]
idx.Pch   = 1:H;
idx.Pdis  = H + (1:H);
idx.SOC   = 2*H + (1:H);
idx.Pgrid = 3*H + (1:H);
nx        = 4*H;

%% Objective function
% Minimize cost + SOC incentive
f = zeros(nx,1);
for k = 1:H
    f(idx.Pgrid(k)) = price_h(k) * dt;
    f(idx.SOC(k))   = f(idx.SOC(k)) - params.c_SOC;
end

%% Variable bounds
lb = zeros(nx,1);
```

```
ub = inf(nx,1);

lb(idx.Pch)   = 0;              ub(idx.Pch)  = params.Pch_max;
lb(idx.Pdis)  = 0;              ub(idx.Pdis) = params.Pdis_max;
lb(idx.SOC)   = params.SOCmin;  ub(idx.SOC)  = params.SOCmax;
lb(idx.Pgrid) = 0;              ub(idx.Pgrid)= inf;

%% SOC dynamics
Aeq = [];
beq = [];

% SOC(k+1) - SOC(k) = -Pch*dt*  /C + Pdis*dt/(  *C)
for k = 1:H-1
    row = zeros(1,nx);
    row(idx.SOC(k+1)) = 1;
    row(idx.SOC(k))   = -1;
    row(idx.Pch(k))   = -dt * params.eta_ch  / params.C;
    row(idx.Pdis(k))  =  dt / (params.eta_dis * params.C);
    Aeq = [Aeq; row];
    beq = [beq; 0];
end

% Initial SOC
row0 = zeros(1,nx);
row0(idx.SOC(1)) = 1;
Aeq = [Aeq; row0];
beq = [beq; SOC_current];

%% End-of-horizon SOC soft constraint (SOC(end) >= SOC_init)
A = [];
b = [];
row_soc_end = zeros(1,nx);
row_soc_end(idx.SOC(end)) = -1;  % -SOC_end <= -SOC_init
A = [A; row_soc_end];
b = [b; -params.SOCinit];

%% Power balance
% Pgrid = Pload + Pch - Pdis - Ppv
Aeq_grid = zeros(H,nx);
beq_grid = zeros(H,1);

for k = 1:H
    Aeq_grid(k, idx.Pgrid(k)) = 1;
    Aeq_grid(k, idx.Pch(k))   = -1;
    Aeq_grid(k, idx.Pdis(k))  =  1;
    beq_grid(k)               = Pload_h(k) - Ppv_h(k);
end

Aeq = [Aeq; Aeq_grid];
beq = [beq; beq_grid];

%% Voltage constraint for first step only
% Vnext = Vbase + (P_batt - P_batt_prev)/S_sen >= 0.955
v_lb = 0.95 + 0.005;
row_volt = zeros(1,nx);
row_volt(idx.Pch(1))  =  1;
row_volt(idx.Pdis(1)) = -1;

b_volt = params.S_sen * (Vbase - v_lb) - P_batt_prev;

A = [A; row_volt];
b = [b; b_volt];

%% Build Gurobi model
model.modelsense = 'min';
model.obj        = f;
model.lb         = lb;
model.ub         = ub;
model.A          = sparse([A; Aeq]);
model.rhs        = [b; beq];
model.sense      = [ ...
```

```
    repmat('<', size(A,1), 1); ...
    repmat('=', size(Aeq,1),1)];

paramsGurobi.OutputFlag     = 0;
paramsGurobi.FeasibilityTol = 1e-6;
paramsGurobi.OptimalityTol  = 1e-6;
paramsGurobi.Method         = 2;

%% Dimension check (safety)
if size(model.A,1) ~= numel(model.rhs)
    error('Constraint count (%d) does not match RHS length (%d).', ...
        size(model.A,1), numel(model.rhs));
end

%% Solve
try
    result = gurobi(model, paramsGurobi);

    if isfield(result,'x') && ~isempty(result.x)
        xopt = result.x;

        Pch  = xopt(idx.Pch);
        Pdis = xopt(idx.Pdis);
        SOC  = xopt(idx.SOC);

        % First-step dispatch
        P_batt = Pdis(1) - Pch(1);

        % SOC consistency warning
        if SOC(end) < params.SOCinit - 1e-6
            warning('End-of-horizon SOC violated: %.3f < %.3f', ...
                SOC(end), params.SOCinit);
        end
    else
        P_batt = 0;
        warning('Gurobi returned empty solution.');
    end

catch ME
    warning('Gurobi solver failed: %s', ME.message);
    P_batt = 0;
end

%% Final safety clipping
P_batt = max(-params.Pch_max, min(P_batt, params.Pdis_max));

end
```

## B.3. Schematic overview of Simulink model

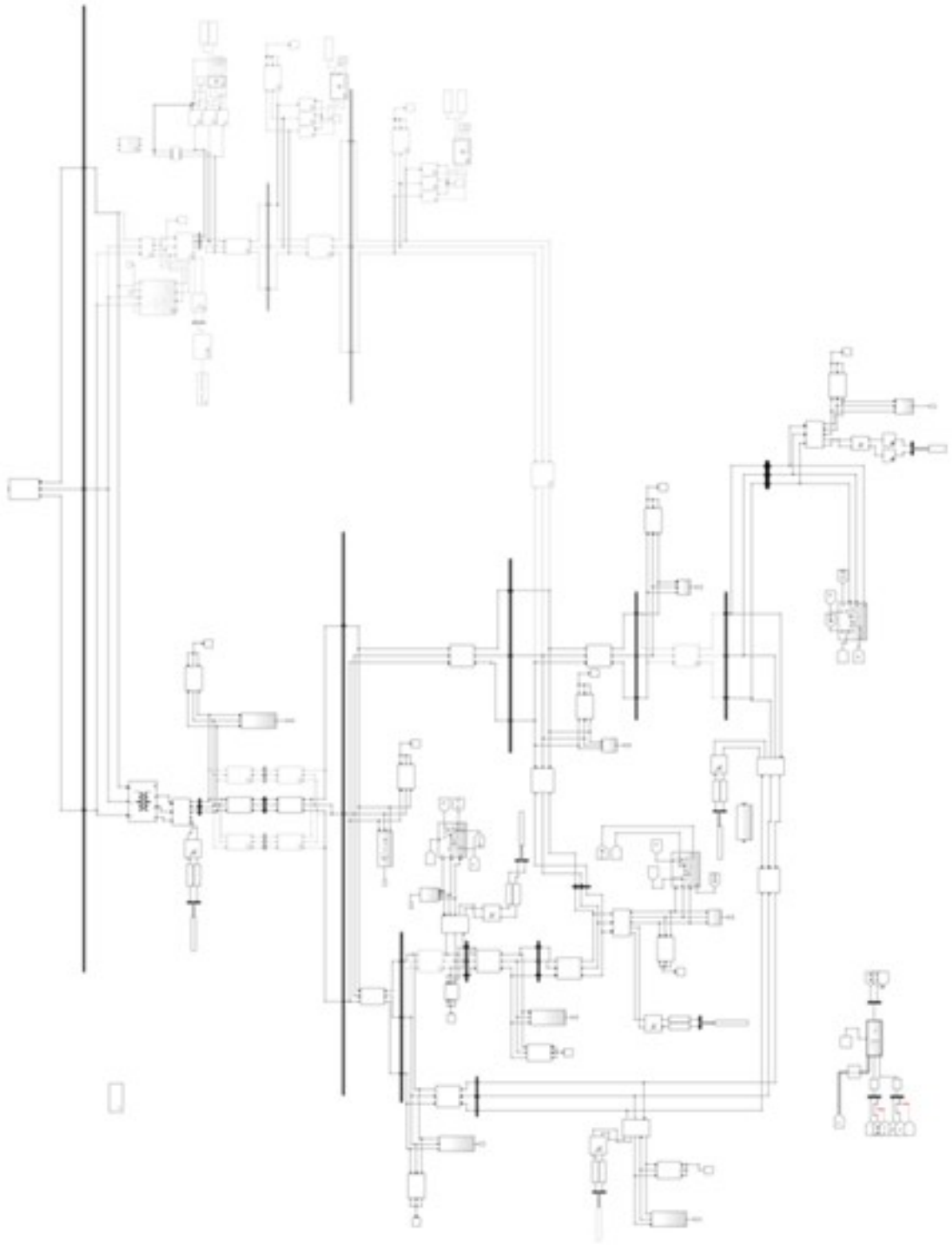

**Figure B.1**